HOKKAIDO UNIVERSITY

Title	Distribution of vertical diffusivity coefficient and water mass formation in the Bussol' Strait : A mixing hot spot in the North Pacific
Author(s)	小野, 数也
Degree Grantor	北海道大学
Degree Name	博士(環境科学)
Dissertation Number	乙第6899号
Issue Date	2013-12-25
DOI	https://doi.org/10.14943/doctoral.r6899
Doc URL	https://hdl.handle.net/2115/54670
Type	doctoral thesis
File Information	Kazuya_Ono.pdf

Hokkaido University Collection of Scholarly and Academic Papers : HUSCAP

博 士 論 文

Distribution of vertical diffusivity coefficient and water mass formation in the Bussol′ Strait: A mixing hot spot in the North Pacific

（北太平洋域における混合のホットスポット、
ブッソル海峡での鉛直拡散係数の分布と水塊形成）

Graduate School of Environmental Science, Hokkaido University

北海道大学大学院環境科学院

Kazuya Ono

小 野　数 也

December, 2013

Abstract

Water mass exchange between the Sea of Okhotsk and the Pacific occurs through the Kuril Straits, which is thought to be a possible site of strong vertical mixing due to tidal current. Strong vertical mixing in the Kuril Straits is believed to be an important contribution to the ventilation of the intermediate layer ($> 27.1\,\sigma_\theta$) and water mass formation ($\sim 26.8\,\sigma_\theta$) in the North Pacific. Furthermore, numerical model studies have suggested that vertical diffusivity in the Kuril Straits is a key factor in the determination of thermohaline circulation in the North Pacific.

The Bussol′ Strait is the deepest (sill depth of 2400 m) and widest (width of 80 km) strait of the Kuril Straits and is thought to be the main exit of water masses from the Sea of Okhotsk to the Pacific. Some studies have also suggested that the outflow from the Sea of Okhotsk through the Bussol′ Strait influences the Oyashio Water and North Pacific Intermediate Water (NPIW). Furthermore, this strait is an important site for water mass formation due to strong tidal mixing caused by the strong diurnal tidal current. Although several observation campaigns have been conducted at the Bussol′ Strait, in all these observations, the mean current with removal of tidal components could not be measured and the observed water mass was inevitably affected by the tidal currents: a different water mass was observed at different tidal periods.

Here we report the distribution of water mass properties in the Bussol′ Strait, the main conduit of water exchange and a possible central site of strong mixing in the Kuril Straits. Our analysis is based on a set of intensive CTD observations in the Bussol′ Strait with a total of 127 casts in summer of 2001. On the basis of these data and all the available historical data, we have revealed the outflow from the Bussol′ Strait to the Pacific and

the significant diapycnal mixing in the strait. In the range 27.0–27.3 σ_θ, the water mass property in the Bussol′ Strait is almost identical to that of the Kuril Basin Water (KBW). The KBW out of the Bussol′ Strait forms a water mass front with the East Kamchatka Current Water (EKCW). This front also corresponds to the front of the Oyashio Current. In the lower part of the intermediate layer (27.3–27.6 σ_θ), part of the water in the strait is characterized by lower temperature, lower salinity, and higher dissolved oxygen than that of KBW and EKCW, which can be explained only by diapycnal mixing. Vigorous diapycnal mixing in the strait can also be shown by the density inversion, occurrence frequency of which corresponds well to the amplitude distribution of the diurnal current. In the density range 26.7–26.8 σ_θ, the water in the Bussol′ Strait has the lowest potential vorticity, suggesting that it is a source region of the low potential vorticity water. Seasonal change of the water can reach up to a density of 26.8 σ_θ around the strait. This leads us to propose that the combination of winter convection and local tidal mixing leads to effective ventilation of the intermediate layer.

Recent observational study has used a microstructure profiler to try to measure vertical mixing directly in the Bussol′ Strait. These observations made in the strait in 2006 and 2007 with repeated casts over 24-hour periods to resolve the mean and tidal components. However, the observations were conducted at a single station hence not necessarily representative of the mean features of turbulence in the Bussol′ Strait. We here estimated the distribution of vertical mixing in the Bussol′ Strait based on indirectly method that is based on the density inversions of all the CTD data taken by *XP01*, with the focus being on vertical structure. We found that vigorous density inversions occurred in the strait with the largest vertical displacement being over 250 m. We estimated the vertical diffusivity coefficient K_ρ from the Thorpe scale for all the CTD data. The vertical average of K_ρ estimated from all the casts is $60 \times 10^{-4}\,m^2\,s^{-1}$. Overall, K_ρ is relatively small in the upper 300 m (density range approximately 26.5–26.7 σ_θ), whereas it is relatively large below a depth of 500 m (density range of $> 26.8\,\sigma_\theta$), with a maximum at the depths of 1100–1700 m. The distributions of K_ρ and the amplitude of the diurnal tidal current are

similar, suggesting that the mixing is caused by the strong diurnal tidal current. The amplification of the diurnal (tidal) current over slopes near the bottom causes the K_ρ maximum at depths of ∼1100–1700 m. We also introduce an empirical relationship between K_ρ and the amplitude of the diurnal tidal current. The vertical diffusivity is one order of magnitude larger at the spring tide than at the neap tide, suggesting that there is extremely large variability of tidal mixing with the fortnightly modulation. In the intermediate layer at densities of 27.3–27.6 σ_θ, large K_ρ values ($> 60 \times 10^{-4}\,\mathrm{m^2\,s^{-1}}$) corresponds well to the colder and less-saline water mass characterized in the Bussol′ Strait, confirming that water mass transformation occurs locally in the strait through strong diapycnal mixing.

Contents

1 General Introduction **1**

2 Water mass exchange and diapycnal mixing in the Bussol′ Strait revealed by water mass properties **11**

2.1 Introduction 11

2.2 Data and method 13

2.3 Result 16

2.3.1 Water mass properties in the Bussol′ Strait 16

2.3.2 Front of the water mass near the Bussol′ Strait 18

2.3.3 Water exchange and mixing inferred from the retrospective data . . 19

2.4 Summary and discussion 21

Figures in Chapter2 36

3 Distribution of vertical diffusivity in the Bussol′ Strait: A mixing hot spot in the North Pacific **37**

3.1 Introduction 37

3.2 Data and methods 40

3.3 Results 43

3.4 Discussion 47

Figures in Chapter3 61

4 General summary and conclusion **61**

Appendix A **65**

Appendix B **69**

Appendix C **71**

Acknowledgments **73**

References **75**

Chapter 1

General Introduction

North Pacific Intermediate Water (NPIW) is characterized by a salinity minimum centered at a density of $26.8\sigma_\theta$ and spreads to the entire subtropical Pacific (Reid, 1973; Talley, 1993). This water contains an anthropogenic compounds such as CO_2 and chlorofluorocarbon (CFC) (Tsunogai et al., 1993; Warner et al., 1996; Ono et al., 2000), although the density surface of $26.8\sigma_\theta$ does not outcrop to the atmosphere within the open North Pacific, even in winter (Reid, 1965). The Sea of Okhotsk is a possible region for ventilation of intermediate water in the North Pacific, including NPIW (Talley, 1991; Warner et al., 1996; Yasuda, 1997). Ventilation of NPIW is derived from sinking of surface water related to high sea-ice production with brine rejection in coastal polynyas along the northern shelf region of the Sea of Okhotsk (Shcherbina et al., 2003).

Including the ventilated water, water mass exchange between the Sea of Okhotsk and the Pacific occurs at the Kuril Straits. The Bussol′ Strait is the deepest and widest strait of the Kuril Straits (Fig. 1.1) and has been considered to be the main exit of the Okhotsk Sea water. In fact, most surface drifters (Ohshima et al., 2002) and profiling floats (target depth of 500–700 m; Ohshima et al., 2010) deployed in the Sea of Okhotsk flowed out into the North Pacific through the Bussol′ Strait during the winter. Based on Lowered Acoustic Doppler Current Profiler (LADCP) observations, Katsumata et al. (2004) have revealed the net transport being from the Sea of Okhotsk to the Pacific (Fig. 1.2).

On the other hands, the Kuril Straits is also an important site for water mass transformation due to strong tidal mixing. Wong et al. (1998) have showed a mixing model

that the CFC concentrations in the Sea of Okhotsk below 27.1 σ_θ cannot be explained only by isopycnal mixing between Dense Shelf Water (DSW) and Pacific water. Thus, they have suggested that diapycnal mixing in the Kuril Straits is the primary contributor to the ventilation in the density range of $> 27.1\,\sigma_\theta$. The water mass with a density of about $26.8\sigma_\theta$ has the largest thickness and thus the lowest potential vorticity in the Sea of Okhotsk (Yasuda, 1997; Itoh et al., 2003). In this density range, the Sea of Okhotsk is suggested as a possible source of the low potential vorticity of NPIW (Yasuda, 1997; Watanabe and Wakatsuchi, 1998). Nishioka et al. (2013) have examined the basin-scale vertical section of dissolved Fe that is originating from the northwestern continental shelf in the Sea of Okhotsk. They have found the very high integrated dissolved Fe concentrations in the water column at the Bussol′ Strait (Fig. 1.3), i.e., the redistribution of Fe water by strong vertical mixing occurs in the Kuril Straits. Therefore, tidal mixing in the Kuril Straits plays a pivotal role for determining the dissolved Fe distribution in the North Pacific region.

Some numerical modelings have estimated the strength of vertical mixing in the Kuril Straits (e.g., Nakamura and Awaji, 2004; Tanaka et al., 2007, 2010a). Tanaka et al. (2010a) mapped the vertically averaged K_ρ around the Kuril Straits, based on a physical model using tidal elevation from TOPEX/POSEIDON altimeter data (Fig. 1.4). Furthermore, anticyclonic eddies have been frequently observed near the Bussol′ Strait (Bulatov et al., 1999; Ohshima et al., 2005), and they are likely caused by baroclinic instability associated with strong tidal mixing (Nakamura and Awaji, 2004; Ohshima et al., 2005). Nakamura and Awaji (2004), using a numerical model, have demonstrated the eddy-like structures of sea surface (~ 15 m) temperature in the vicinity of Kuril Straits(Fig. 1.5). On the other hands, several investigations have suggested that strong vertical mixing in the Kuril Straits has a significant influence on the water mass distributions and thermohaline circulation in the North Pacific (Tatebe and Yasuda, 2004; Nakamura et al., 2006; Kawasaki and Hasumi, 2010). Nakamura et al. (2006), on the basis of a general circulation model, have shown the enhanced ventilation of NPIW in case that strong vertical mixing is given at

the Kuril Straits (Fig. 1.6). Kawasaki and Hasumi (2010), using both a general circulation model and a box model, have also suggested that the structure of meridional circulation cells in the North Pacific may be particularly sensitive to the vertical profile of the vertical diffusivity coefficient K_ρ in the Kuril Straits. When strong vertical mixing from the deep layer reaches the sea surface, localized upwelling occurs in the Kuril Straits, resulting in a single meridional circulation cell in the North Pacific (Fig. 1.7a). On the contrary, when strong mixing does not reach the surface, downwelling occurs in upper layers, resulting in double circulation cells (Fig. 1.7b).

Several observations have been performed in the Bussol′ Strait (Kono and Kawasaki, 1997; Riser, 2001; Yasuda et al., 2002). Although, these observations could not provided the mean current with removal of tidal components and a different water mass was observed at different tidal periods. To discuss the water mass property under the vigorous tidal exchange flow in the strait, we need repeated observations to resolve the mean and tidal components. To resolve the mean and tidal components, intensive observations were conducted across the Bussol′ Strait aboard the Research Vessel *Prof. Khromov* in 2001 (hereafter *XP01*), using a Lowered Acoustic Doppler Current Profiler (LADCP) and Conductivity Temperature Depth (CTD) profiler.

The first topic of the dissertation is to reveal the features of water mass exchange between the Sea of Okhotsk and the Pacific through the Bussol′ Strait based on *XP01* data as described in Chapter 2. Furthermore, we find where intensive diapycnal mixing likely occurs in and around the Bussol′ Strait and suggest that such diapycnal mixing in the strait plays an important role in water mass formation. The result of *XP01* only gives us a snapshot feature, hence we create a climate data set to confirm the water mass exchange and mixing in and around the Bussol′ Strait.

The second topic of the dissertation is to estimate the vertical diffusivity in the Bussol′ Strait on the basis of *XP01* data as described in Chapter 3. Recent observation studies have used a microstructure profiler to try to measure vertical diffusivity directly in the Kuril Straits (e.g. Itoh et al., 2010, 2011; Yagi and Yasuda, 2012). Yagi and Yasuda

(2012) have made direct observations of turbulent mixing using a VMP-2000 profiler at one station in the Bussol′ Strait in 2006 and 2007 (Fig. 1.8). In contrast, the *XP01* data did not involve direct observations of turbulence, but conducted intensive CTD and LADCP observations across the strait. If these CTD or LADCP data can provide indirect information of the vertical mixing, the data set could be a potentially valuable data set for mapping of the vertical diffusivity in the strait. Therefore, we adopt an indirect method to estimate the distribution of vertical diffusivity in the strait using CTD data taken by *XP01*. Finally, summary of this dissertation is given in Chapter 4.

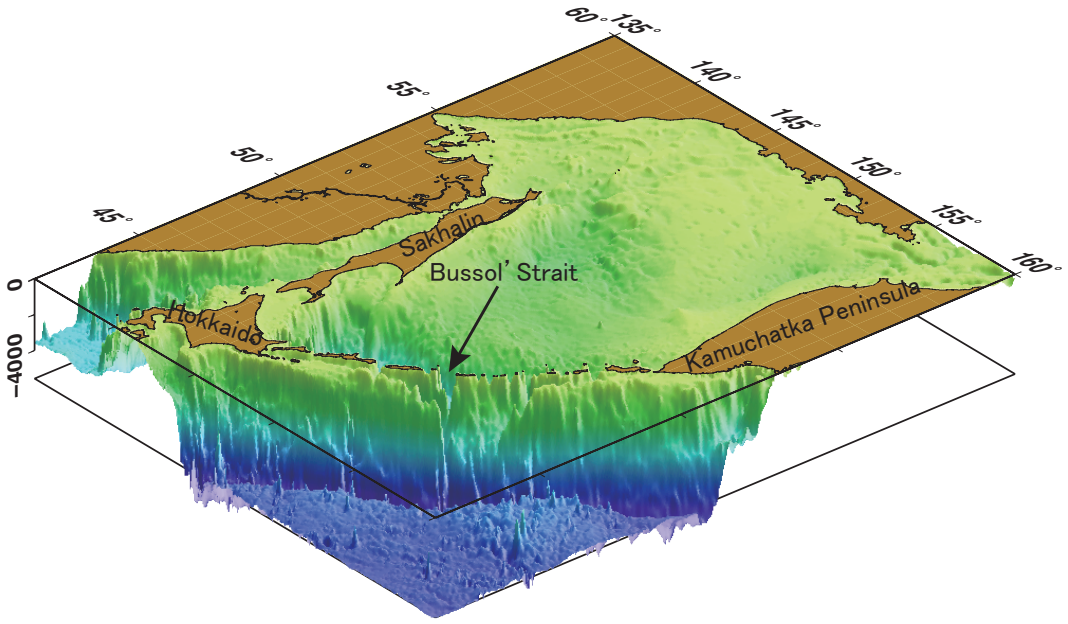


Figure 1.1 3D bathymetry around the Kuril Island Chain. Bathymetry data are derived from the gridded data by ETOPO2.

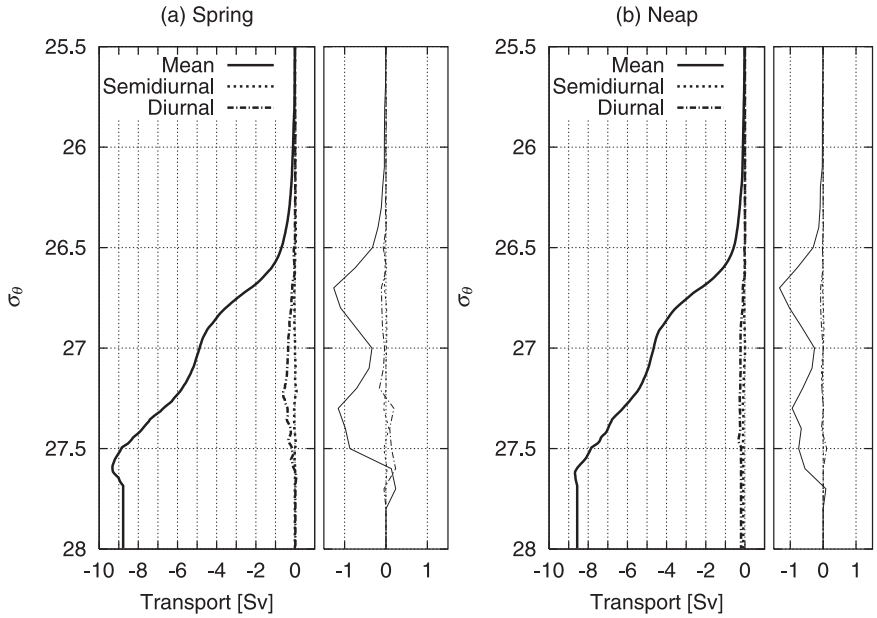


Figure 1.2 Transport as a function of potential density for the (a) spring and (b) neap tides. Thin lines show transport at intervals of 0.1 σ_θ. Thick lines show transport integrated from the surface to the bottom. Negative values denote the transport from the Sea of Okhotsk to the Pacific. This figure is cited from Katsumata et al. (2004).

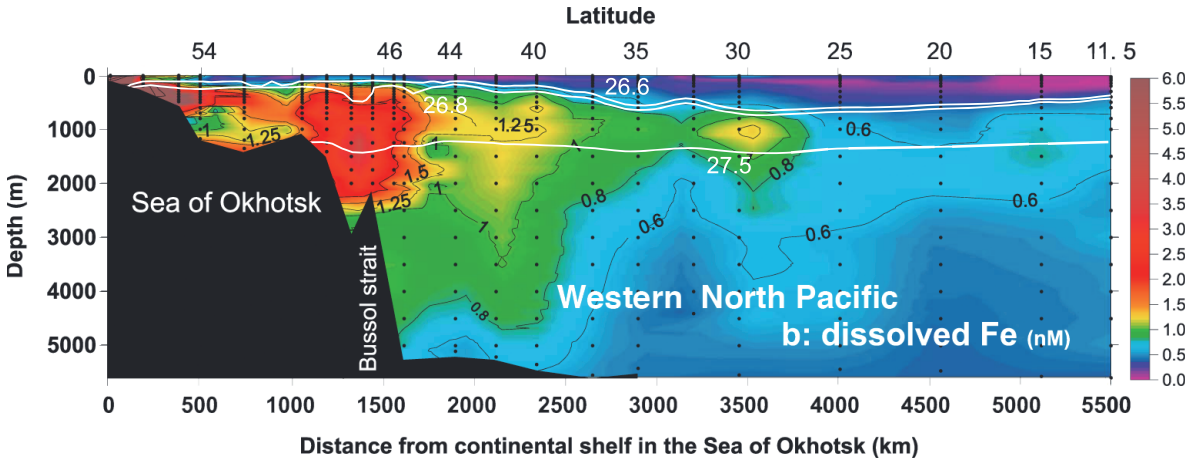


Figure 1.3 Vertical section profile of dissolved Fe, starting in the Sea of Okhotsk, passing through the Bussol′ Strait, then heading south along 155° E from the subarctic to the tropics. Isopycnal surfaces are also shown by the white contour lines of 26.6, 26.8, and 27.5 σ_θ. This figure is cited from Nishioka et al. (2013).

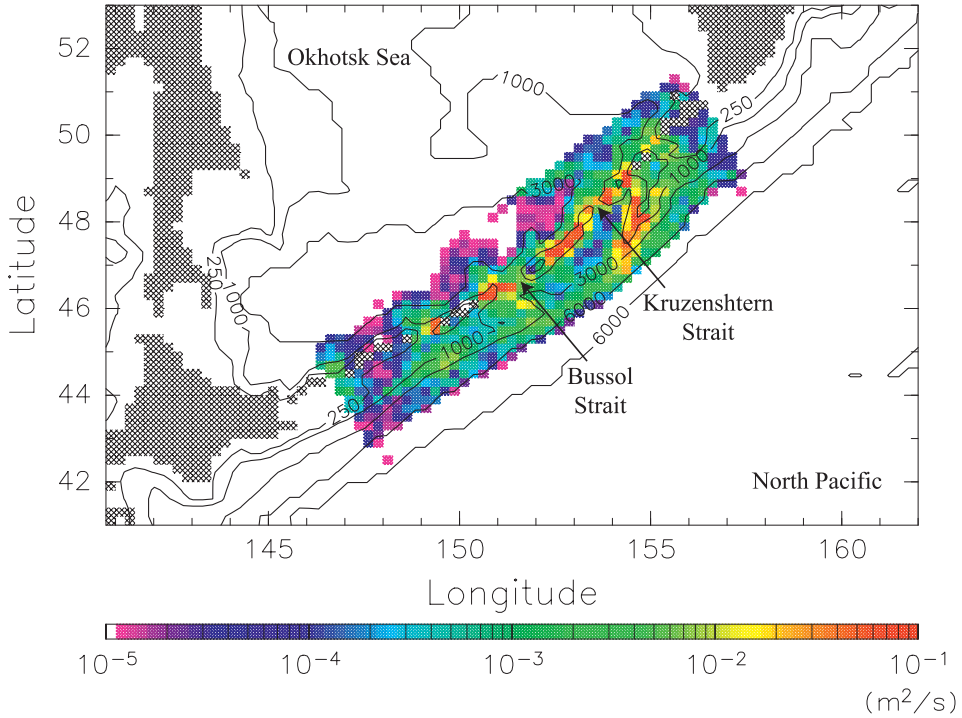


Figure 1.4 Distribution of vertically averaged diapycnal diffusivity based on a barotropic tidal model fitted by tidal elevation from TOPEX/POSEIDON altimeter data (Tanaka et al., 2010a).

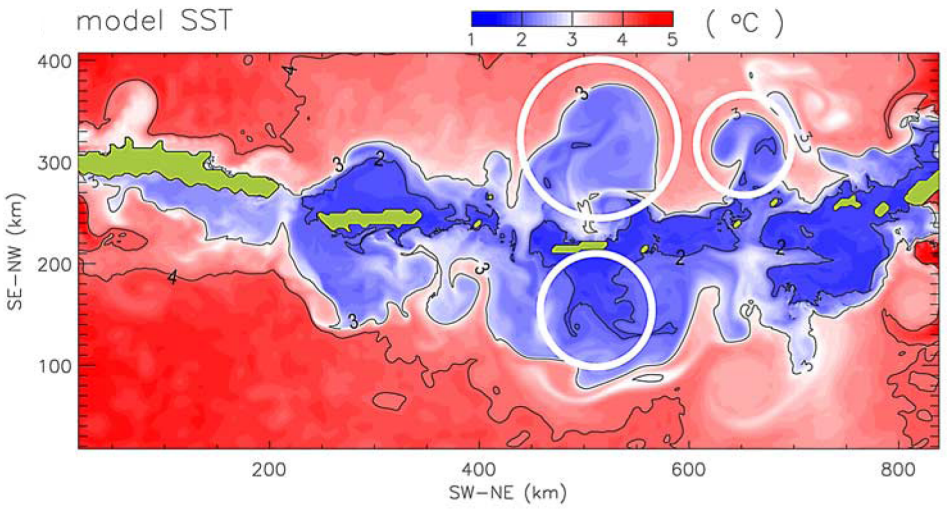


Figure 1.5 Sea surface temperature snapshot along the Kuril Island Chain, using a three-dimensional nonhydrostatic model by Nakamura and Awaji (2004). White circles indicate eddy-like structures also seen in satellite-derived sea surface temperature imagery.

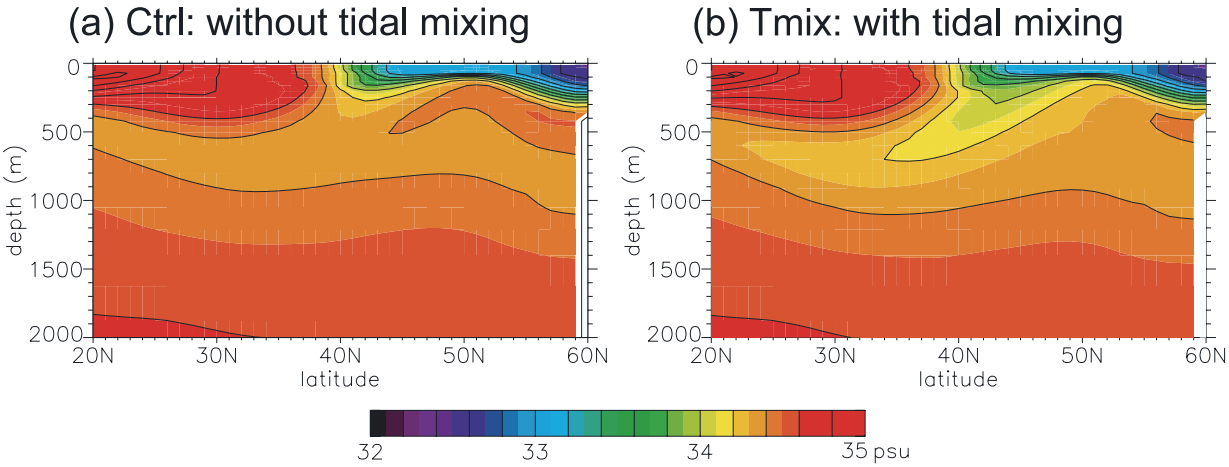


Figure 1.6 Sensitivity of the NPIW formation to vertical diffusivity given in the Kuril Straits. Meridional sections of salinity are shown at 165 °E in the North Pacific region. The given K_ρ over the sills in the Kuril Straits are shown for (a) not increased and (b) increased by $200 \times 10^{-4}\,\mathrm{m^2\,s^{-1}}$ case. Adopted from Nakamura et al. (2006).

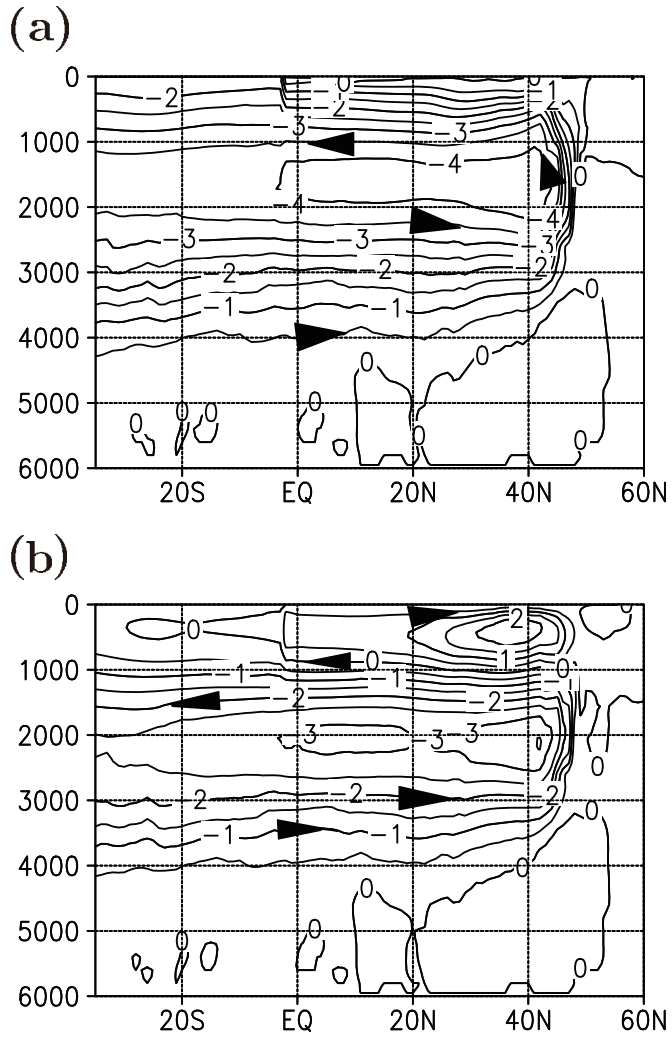


Figure 1.7 Sensitivity of the structure of thermohaline circulation to vertical diffusivity given in the Kuril Straits. Black arrows indicate difference of the Pacific meridional circulation stream function from background case: there is not locally enhanced vertical mixing in the Kuril Straits. The given K_ρ in the Kuril Straits are shown for (a) uniformly strong vertical diffusivity from surface to bottom ($200\,cm^2/s$) and (b) weak vertical diffusivity in the upper layer ($0.2\,cm^2/s$) and strong one in the lower layer ($200\,cm^2/s$). Adopted from Kawasaki and Hasumi (2010).

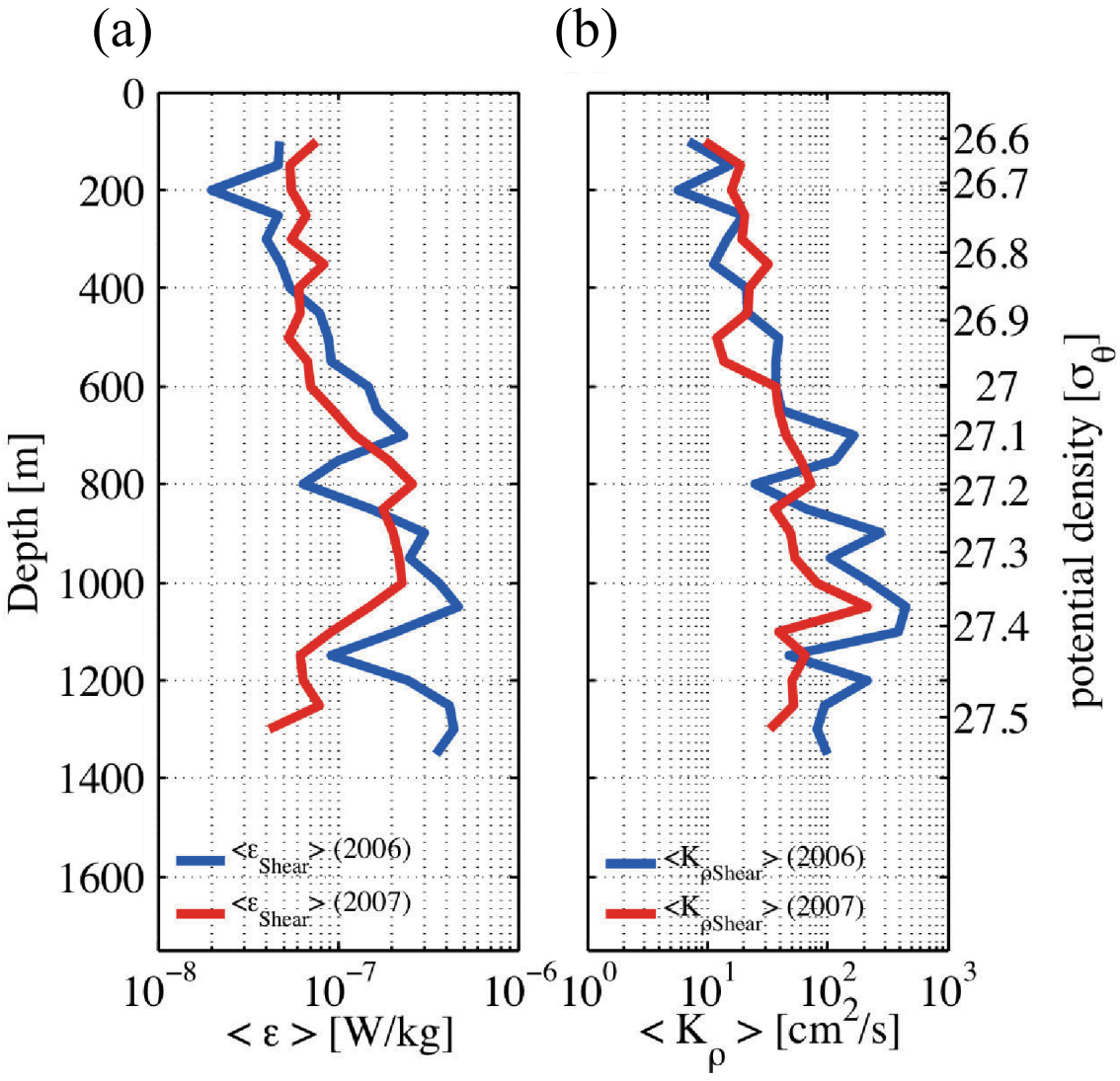


Figure 1.8 Vertical profiles of 1-day-averaged (a) ϵ and (b) K_ρ at one station (close to Station F1) in the Bussol′ Strait in 2006 and 2007, using a VMP-2000 data. Adopted from Yagi and Yasuda (2012).

Chapter 2

Water mass exchange and diapycnal mixing in the Bussol′ Strait revealed by water mass properties

2.1 Introduction

The North Pacific Intermediate Water (NPIW) is characterized by a salinity minimum at a density of around 26.8 σ_θ (Reid, 1965) and widely distributed at intermediate depth over the North Pacific region (Reid, 1973; Talley, 1993). The Sea of Okhotsk is the only location where the density surface of the NPIW outcrops to the atmosphere within the North Pacific region. It is also the only location for ventilation of the NPIW, which in turn may induce the ventilation of anthropogenic compounds such as CO_2 and CFC (Warner et al., 1996; Wong et al., 1998; Ono et al., 2000; Andreev et al., 2001; Yasuda et al., 2002).

The Okhotsk water, including the ventilated water, exchanges with the Pacific water through the Kuril Straits. The Bussol′ Strait, which is the largest and deepest strait in the Kuril Straits, is thought to be a main conduit for the outflow from the Sea of Okhotsk to the Pacific. The fact that most of the surface drifters deployed in the Sea of Okhotsk flowed out to the North Pacific through the Bussol′ Strait suggests that the strait is the main pathway by which the surface water flows out from the Sea of Okhotsk (Ohshima et al., 2002). Other studies have also suggested that the outflow from the Sea of Okhotsk through the Bussol′ Strait influences the Oyashio Water and NPIW (Talley, 1991; Yasuda,

1997; Yasuda et al., 2002; Itoh et al., 2003). On the other hand, it is indirectly suggested that the water exchange in the Bussol′ Strait has a two-layered feature, with the upper layer flowing toward the Pacific and the lower flowing in the opposite direction (Kobayashi, 2000).

The Bussol′ Strait is an important site, not only for the main passage between the Sea of Okhotsk and the Pacific but also for water mass transformation due to strong tidal mixing. From surface drifter data strong amplification of both diurnal and semi-diurnal tidal currents were observed in and around the Bussol′ Strait, even in regions deeper than 2000 m (Ohshima et al., 2002). Nakamura and Awaji (2004), using a numerical tidal simulation model, suggested that tidal currents are amplified over the Bussol′ Strait and that the vertical turbulent mixing and diffusion become very large over the sills, with vertical diffusivity values reaching 10–50 $\mathrm{cm^2\,s^{-1}}$, especially near the bottom. Furthermore, the intense diapycnal mixing leads to eddies by baroclinic instability associated with the near-surface front in the region between the enhanced mixing and offshore regions (Ohshima et al., 2005; Nakamura and Awaji, 2004).

Conventional geostrophic calculations are not available around the straits because the flow cannot be in geostrophic balance due to the dominance of the strong tidal current (Riser et al., 1995). Although several observation campaigns have been conducted at the Bussol′ Strait (Kawasaki and Kono, 1994; Yasuda, 1997; Kono and Kawasaki, 1997; Riser, 2001; Yasuda et al., 2002), in all these observations, the mean current with removal of tidal components could not be measured and the observed water mass was inevitably affected by the tidal currents: a different water mass was observed at different tidal periods. To discuss the water mass property as well as the exchange flow at the strait, we need repeated observations to resolve the mean and tidal components.

In 2001, under the international Japan-Russia-United States joint study of the Sea of Okhotsk, repeated casts of a Lowered Acoustic Doppler Current Profiler (LADCP) and a Conductivity-Temperature-Depth profiler (CTD) were performed at 13 stations that cross the narrowest part of the Bussol′ Strait. Time series covering more than at least

24 hours were obtained for each station, and thus the mean, diurnal, and semidiurnal components may be resolved to some degree. These observations provided the mean velocity, temperature, and salinity data at the Bussol′ Strait for the first time. Katsumata et al. (2004), using the LADCP data of these observations, revealed the mean exchange flow and the tidal current characteristics at the strait. They showed that, in the mean component, the upper part (26.5–27.5 σ_θ) flows toward the Pacific while the lower part ($\sigma_\theta > 27.5$) flows in the opposite direction with a net transport of ~ 9 Sv ($1\,\mathrm{Sv} = 10^6\,\mathrm{m^3\,s^{-1}}$) (Fig. 1.2). In other words, the flows show a two-layered feature. Katsumata et al. (2004) also showed that the diurnal tidal current reaches an amplitude of more than $1.0\,\mathrm{m\,s^{-1}}$ in the western channel of the strait, even at depths below 1000 m.

In this chapter we reveal the features of water mass exchange between the Sea of Okhotsk and the Pacific through the Bussol′ Strait, based on 127 casts of the CTD data taken on the Research Vessel *Prof. Khromov* in 2001 (*XP01*). Furthermore, we show that intensive diapycnal mixing likely occurs in some layers in and around the Bussol′ Strait and suggest that such diapycnal mixing in the strait plays an important role in water mass transformation. The chapter discusses the water exchange through the Bussol′ Strait in terms of water mass analysis. The companion paper by Katsumata et al. (2004) discusses water exchange through the strait in terms of direct current measurements with LADCP. The result of *XP01* only gives us a snapshot feature, hence we take a retrospective approach to the water exchange and mixing in and around the Bussol′ Strait, based on all available historical data.

2.2 Data and method

Intensive observations with LADCP and CTD were performed in the Bussol′ Strait from 31 August 2001 to 12 September 2001 on board the R/V *Prof. Khromov*. Repeated observations were done at 13 stations (A1, A2, B1, B2, B3, C1, C2, D1, D2, E1, E2, F1, and F2: see Fig. 2.1 for the locations) with a total of 127 casts (actually 254 including up and down casts). To resolve the mean and tidal components, more than six casts

(actually 12 including up and down casts) over a period of over 24 hours were done at each station. There are two deep channels in the Bussol′ Strait (see the bottom contours in Figs. 2.1 and 2.12). Since a large part of the water exchange is likely to occur around the deep channels, observation was done at both spring and neap tides in the two deep channels. Details of the observational design were described in Katsumata et al. (2004).

Hydrographic observations were done using the Seabird SBE-911 plus CTD system manufactured by SeaBird Electronics, Inc. The accuracy of the CTD is 0.002 °C for temperature, 0.0003 mmho cm^{-1} (0.002 psu) for conductivity, and 0.015% for depth. The CTD was equipped with Beckman-type polarographic dissolved oxygen sensors: SBE-13B. A supplementary observation was done with the expendable CTD (XCTD) manufactured by Tsurumi Seiki Co., Ltd. Original CTD data were interpolated to 1 dbar interval data. The salinity data from the CTD were calibrated with water samples measured by the AUTOSAL salinometer. Dissolved oxygen data were calibrated by the autotitration machine COM-450 manufactured by Hiranuma Sangyo Co., Ltd. The XCTD can measure temperature and salinity profiles down to 1000 m, with accuracies of 0.02 °C for temperature, 0.03 mS cm^{-1} for conductivity, and 5 m or 2% for depth. Current measurements were done using the 300 kHz broadband LADCP manufactured by RD Instruments.

In addition to the analysis of *XP01* data, we have created a retrospective data set in the region around the Bussol′ Strait from all available hydrographic data (see Fig. 2.2 for locations). The data set consists of the World Ocean Database 2001 (WOD01) from the National Oceanographic Data Center (NODC) and JODC Data On-line Service System (J-DOSS) from the Japan Oceanographic Data Center (JODC). Besides these online data, our data set includes CTD and XCTD data obtained by the R/V *Prof. Khromov* from 1998 to 2001, by the R/V *Kaiyo-Maru* of the Japan Fisheries Agency in 1996, and profiling float data. The resulting data set is 17% larger than that extracted from the online data. From these data, we constructed maps of the potential temperature, salinity, and dissolved oxygen content on potential density surfaces in the density range of 26.6–27.4 σ_θ. We adopted isopycnal averaging rather than depth averaging because water mixing would

occur preferentially along a constant density surface, except for the event of regional tidal mixing. It is also noted that, for the intermediate layers, the isopycnal surfaces in the North Pacific are about 100 m shallower than those in the Sea of Okhotsk. Thus, the isopycnal averaging data set seems more appropriate than the depth averaging set for describing the distributions of water properties. Before the construction of the gridded data set, we manually excluded low-quality data, those having abnormal temperature or salinity from temperature-salinity relations, as well as those showing unrealistic profiles. All the oxygen content data prior to 1960 were excluded because the oxygen titration method changed in the mid-1950s (Lozier et al., 1995). A total of 8% of all data were excluded.

Bottle sampling data of potential temperature, salinity and dissolved oxygen content in WOD01 were linearly interpolated onto 1 dbar intervals. The interpolated data of the potential temperature and dissolved oxygen were averaged over $\pm 0.025\,\sigma_\theta$ density range at selected isopycnals (26.6, 26.8, 27,0, 27.2, and $27.4\sigma_\theta$). We constructed a gridded data set from these isopycnal data. Grid spacing of $0.2^\circ \times 0.3^\circ$ latitude-longitude were taken for potential temperature using the Gaussian distribution as a weight function with the e-folding scale and influence radius of 30 km. Our focus lies on the region around the Bussol′ Strait, where we have a relatively large number of data obtained by the R/V *Prof. Khromov* from 1998 to 2001. For this region, enclosed by the solid lines in Fig. 2.2, grid spacing of $0.1^\circ \times 0.15^\circ$ latitude-longitude was taken for potential temperature with the e-folding scale and influence radius of 20 km. For grid cells with no data or fewer than three observations within the influence radius, that grid cell is regarded as a deficit cell.

2.3 Result

2.3.1 Water mass properties in the Bussol′ Strait

Figure 2.3 shows the distribution of occurrence frequencies on the potential temperature and salinity diagram calculated from all the CTD data in the Bussol′ Strait during *XP01* cruise. Figure 2.3 also presents the potential temperature-salinity relation of two water masses which can be ingredients of the water in the Bussol′ Strait: one is the East Kamuchatka Current Water (EKCW: green lines) and the other is the Kuril Basin Water (KBW: blue lines). To calculate the two water mass properties, we adopted 159 and 84 CTD station data for KBW and EKCW, respectively (see Fig. 2.1a for locations of the stations).

The intermediate layer (26.8–27.6 σ_θ) in the Bussol′ Strait can be classified into three layers in terms of water mass properties. In the upper part (26.8–27.0 σ_θ) of the intermediate layer, the water mass property in the Bussol′ Strait lies in between those of KBW and EKCW. In the middle part (27.0–27.3 σ_θ), the property is similar to that of KBW. In the lower part (27.3–27.6 σ_θ, see the enlargement of Fig. 2.3b), in addition to KBW and EKCW, there is a water mass that has lower temperature and salinity than both KBW and EKCW. This water property cannot be explained by simple isopycnal mixing between the two water masses. We examined all the available data from high resolution CTD and profiling floats, and confirmed that, around 27.4 σ_θ, no water having lower temperature and salinity than that in the strait exists in other areas of the Sea of Okhotsk and the nearby Pacific. This property can be explained only by diapycnal mixing between adjacent layers, suggesting that in the density range of 27.3–27.6 σ_θ, significant vertical mixing across density surfaces occurs locally in the strait. Below the intermediate layer (density greater than 27.65 σ_θ), the difference in property is very small among KBW and EKCW, and the water in the strait.

Figure 2.4 shows the occurrence frequency distribution of the dissolved oxygen content versus potential density in the Bussol′ Strait from all the *XP01* data. For comparison, the dissolved oxygen contents of KBW and EKCW are superimposed in Fig. 2.4. In the

surface layer (density smaller than 26.6 σ_θ), the dissolved oxygen is overall lower than that of KBW and EKCW. This likely results from stronger upward transport of water with low dissolved oxygen content from the lower layer due to diapycnal mixing in the strait. In the density range of 26.8–27.3 σ_θ, as in the potential temperature-salinity relation, the dissolved oxygen content in the strait shows a similar value to that of KBW. In the density range of 27.3–27.5 σ_θ, part of the water in the strait shows a higher value than that of KBW and EKCW, which might suggest the existence of diapycnal mixing in this density range.

Figure 2.5 shows the occurrence frequency distribution of the potential vorticity ($Q = -(f/\rho)(\partial\sigma_\theta/\partial z)$) versus potential density in the Bussol′ Strait, where f is the Coriolis parameter, ρ is the density, and $\partial\sigma_\theta/\partial z$ is the vertical gradient of potential density. The Sea of Okhotsk is suggested as a source of low potential vorticity of NPIW at around 26.8 σ_θ (Yasuda, 1997; Watanabe and Wakatsuchi, 1998). Also in Fig. 2.5, the potential vorticity profiles of KBW are superimposed, showing that most of them have a minimum value around 26.7–26.8 σ_θ. The potential vorticity in the strait from 26.7 to 26.8 σ_θ is further lower than that of KBW. In other words, the water volume at this density range is particularly large in and around the Bussol′ Strait. Itoh et al. (2003) showed, from the climatological map of the layer thickness between 26.75–26.85 σ_θ, that the area of largest thickness, thus lowest potential vorticity, is found between the Bussol′ Strait and the Kruzenshtern Straits (see Fig. 2.1a for locations) in the Sea of Okhotsk. The vigorous diapycnal mixing reduces the density gradient of the water column, creating low potential vorticity water. We infer that the low potential vorticity water around 26.8 σ_θ is created by vigorous diapycnal mixing in and around the Bussol′ Strait due to the strong tidal currents around this density range.

To summarize, the following points can be inferred for the water exchange and mixing in the intermediate layer. In the density range of 26.7–27.0 σ_θ (approximately 300–600 m), potential temperature-salinity relation (Fig. 2.3) and potential vorticity profiles (Fig. 2.5) suggest relatively intense diapycnal mixing in the Bussol′ Strait and also the production

of water with density around 26.8 σ_θ. In the density range of 27.0–27.3 σ_θ (approximately 600–1000 m), the Bussol′ Strait area is occupied by KBW. In the density range of 27.3–27.6 σ_θ (approximately 1000–1800 m) part of the water in the strait has lower temperature, lower salinity, and higher dissolved oxygen content than both KBW and EKCW. This supports the hypothesis that the low temperature and salinity water in the strait results from local diapycnal mixing and that the Bussol′ Strait is the main site for diapycnal mixing in the lower intermediate water (27.3–27.6 σ_θ). In deeper water with density greater than 27.65 σ_θ (approximately below 1800 m), the difference is very small in the water mass properties among the Pacific, the Bussol′ Strait, and the Sea of Okhotsk. In this deep layer, the current measurements show an inflow from the Pacific to the Sea of Okhotsk through the Bussol′ Strait (Katsumata et al., 2004). In the deep layer with water denser than 27.65 σ_θ, the Pacific water likely flows into the Sea of Okhotsk through the Bussol′ Strait without significant diapycnal mixing.

2.3.2 Front of the water mass near the Bussol′ Strait

Here we examine the mixing ratio between KBW and EKCW as a function of potential density on the vertical section crossing the Bussol′ Strait from the Sea of Okhotsk to the Pacific, using the *XP01* cruise data (Fig. 2.6). The mixing ratio is given by $(\theta - \theta_{KBW})/(\theta_{EKCW} - \theta_{KBW})$, where θ, θ_{EKCW}, and θ_{KBW} is the potential temperature at a certain potential density for observed water, EKCW, and KBW, respectively. To estimate the mixing ratio, we adopt the representative properties of KBW and EKCW from Fig. 2.3 (solid bold lines). In Fig. 2.6 the smaller value (darker tone) indicates water closer to KBW. The water in the strait, which has a nearly identical property to that of the KBW, extends to the Pacific and forms a water mass front with EKCW, where the extent of KBW is greater in the deeper layer.

In Fig. 2.6, contours of geostrophic velocities relative to 1000 dbar are superimposed by solid lines. Although the absolute velocities cannot be obtained, the core of the Oyashio Current can be identified in the upper layer on the Pacific side. The water mass front (the

position with mixing ratio 0.4–0.6) corresponds well to the velocity front (the position with the geostrophic velocity components being nearly zero).

Figure 2.7a shows the potential temperature-salinity diagram for all the down and up CTD casts taken at Station B5, located on the Pacific side, at a distance of 10 km from the strait (see Fig. 2.1b and Fig. 2.6 for the location). The observations were taken within a day. Nevertheless, the water mass from each cast showed significantly different property for water with densities less than 27.1 σ_θ. Significant differences are found even between the up and down casts of the same observation. These suggest that the position of the water mass front was located near Station B5 and was changing due to the strong tidal currents through the Bussol′ Strait. Here we pay attention to the two casts in which the water mass property is particularly shifted to that of EKCW (designated by red lines in Fig. 2.7a). From the vertical velocity profiles as a function of potential density (Figs. 2.7b and c), when the water mass property shifts to that of EKCW, a southwestward flow of the Oyashio Current or northwestward flow toward the strait tends to appear. This implies that the Oyashio approaches and departs from the strait due to the tidal current across the strait, and correspondingly, the covering area or front of the Oyashio water is changed by the tidal cycle. On the other hand, in the deeper water with density greater than 27.1 σ_θ, the water mass property is nearly identical to that of KBW.

The analyses of this section suggest the following points. The water in the intermediate layer at the Bussol′ Strait, which has a property nearly identical to that of KBW, flows from the Sea of Okhotsk to the Pacific, and then forms the water mass front with EKCW. This water mass front corresponds to the front of the Oyashio Current. The front is advected back and forth near the strait by the strong tidal current.

2.3.3 Water exchange and mixing inferred from the retrospective data

The result in the previous section is based on a snapshot of one-time cruise data. To describe the mean state (more general features) around the Bussol′ Strait, we show the

climatology of the water mass properties on potential density surfaces using all the retrospective hydrographic data.

We examined the climatology of the potential temperature on isopycnal surfaces for March to June (spring: Fig. 2.8a), when a remnant of the winter mixed layer exists, and for July to October (summer: Fig. 2.8b). Comparison of the spring and summer cases show that in the upper layer of $26.6\,\sigma_\theta$, the potential temperature in spring is significantly lower than that in summer, implying the remnant of the winter mixed layer. Paying attention to the area around 46°30' N and 151° E, the temperature is lower in spring and higher in summer than that in the surrounding regions. This suggests that, in this layer, the vertical mixing with the upper layer is particularly strong around this area. A noticeable feature appears on $26.8\,\sigma_\theta$ around the area of the Bussol′ Strait: the temperature is significantly lower in spring than in summer in spite of the fact that winter convection cannot reach this density layer in the North Pacific (Talley, 1991) and the Kuril Basin (Gladyshev et al., 2003). From all the available data from profiling floats from January to March in the Sea of Okhotsk and the Pacific nearby, we found that the winter convection reaches at most $26.7\,\sigma_\theta$ but not $26.8\,\sigma_\theta$ density surface (Fig. 2.9). Our interpretation of the seasonal change in the Bussol′ Strait is as follows. Through the strong diapycnal mixing in the strait, the water deepened by surface cooling in winter but not up to the $26.8\,\sigma_\theta$ density level can be further transported to the lower layer that is not directly ventilated. In this way, the influence of the winter convection reaches down to the $26.8\,\sigma_\theta$ density layer near the strait. In the lower part of the intermediate layer ($27.0\,\sigma_\theta$), no significant difference can be found between spring and summer. The influence of the winter convection appears to reach at most to the upper part of the intermediate layer.

Figure 2.10 shows the horizontal distributions of the mixing ratio between KBW and EKCW (the definition is the same as that of Fig. 2.6) on the isopycnal surfaces to which winter convection cannot reach directly. The Bussol′ Strait is occupied by KBW or the water formed in the strait. The water then extends to the Pacific southward or southwestward in the intermediate layer. The vertical section, with a line similar to that

of Fig. 2.6, is also presented from the retrospective data set in Fig. 2.10e. The structure of the Oyashio front is found to be similar to that of Fig. 2.6.

Finally, we examine the horizontal distributions of the dissolved oxygen content on isopycnal surfaces (Fig. 2.11). Since the data number is too small to produce the gridded data set, raw station data are plotted. Since we could not find any significant seasonal dependence, even at the 26.6 σ_θ surface, we use all the available oxygen data for all seasons. It is found that, at 26.6 and 26.8 σ_θ, the dissolved oxygen around the strait is lower than that in the surrounding regions. This also supports the hypothesis that the diapycnal mixing is particularly strong around the Bussol′ Strait. As explained in Fig. 2.4, the supply of water with low dissolved oxygen content from the lower layer appears to be stronger through the mixing at these density ranges. Down to 27.2 σ_θ, the oxygen content in the Bussol′ Strait does not differ from that in the Kuril Basin and its signal extends to the Pacific southwestward, as in Fig. 2.10.

2.4 Summary and discussion

The water mass analyses based on the extensive CTD observation in *XP01* revealed several features of the water mass exchange through the Bussol′ Strait. In the density range of 27.0–27.3 σ_θ, the property of the water in the Bussol′ Strait is almost identical to that of KBW. The KBW flows out to the Pacific through the Bussol′ Strait and extends to the Oyashio downstream. Such a distribution is also shown from the retrospective data set. This suggests a net outflow from the Sea of Okhotsk to the Pacific in the density range of 27.0–27.3 σ_θ, consistent with the direct flow measurements from the LADCP during the same cruise (Katsumata et al., 2004). The KBW out of the Bussol′ Strait forms a water mass front with EKCW. This front also corresponds to the front of the Oyashio Current. The front is advected back and forth near the strait by the strong tidal current.

Our analyses of water mass properties also suggest that strong vertical mixing occurs in the vicinity of the Bussol′ Strait. Around the Bussol′ Strait, the seasonal change of

water properties can be identified up to the density range of 26.8 σ_θ, to which winter convection cannot reach directly: no signal of outcropping with a density greater than 26.8 σ_θ can be found from all the profiling floats drifting around the strait in winter. Our interpretation of the seasonal change is that the water, deepened by surface cooling in winter but not up to the 26.8 σ_θ density level, is subsequently deepened by the strong diapycnal mixing in the strait up to that density level. We propose that combination of winter convection and strong tidal diapycnal mixing leads to an effective ventilation of the intermediate layer. Through this combination mechanism interannual variability of the winter cooling would possibly penetrate into the intermediate water.

Having a lower potential vorticity (thicker layer) than the North Pacific around the 26.8 σ_θ isopycnal surface, the Sea of Okhotsk is suggested as a source of low potential vorticity (Yasuda, 1997). Our analyses show that potential vorticity in the Bussol′ Strait is further lower than that in the Sea of Okhotsk in the density range of 26.7–26.8 σ_θ. This suggests that the Bussol′ Strait is the specific source region where the low potential vorticity (thicker layer) is formed around this density range due to the local enhancement of vigorous diapycnal mixing.

In the lower part of the intermediate layer (27.3–27.6 σ_θ), part of the water in the strait is characterized by lower temperature, lower salinity, and higher dissolved oxygen than KBW and EKCW. These properties cannot be explained by the isopycnal mixing between KBW and EKCW, but only by diapycnal mixing. Such water can be found only around the Bussol′ Strait, which suggests that the strait plays a major role in diapycnal mixing in the lower part of the intermediate layer. Active diapycnal mixing in the Bussol′ Strait is evidenced by density inversions observed in the *XP01* CTD data. Figure 2.12a shows the vertical distribution of the occurrence frequencies of the density inversion in the Bussol′ Strait from the all *XP01* data. Density inversions are most prominent from the bottom to 300–500 m above the bottom, especially over the slope of the central seamount of the strait. These features correspond well to the distribution of the vertical diffusivity coefficients in the Bussol′ Strait, obtained from a numerical tidal simulation model (Naka-

mura and Awaji, 2004) and that of the amplitude for the diurnal tidal current (Fig. 2.12b) derived from the LADCP data of the *XP01* cruise (Katsumata et al., 2004). These density inversions are likely caused by internal-wave breaking (Nakamura and Awaji, 2004) or boundary mixing near the bottom due to the strong tidal current in the strait, which suggests significant diapycnal mixing even in deep parts of the strait (27.4–27.6 σ_θ).

This chapter only suggests where and in which layer the diapycnal mixing occurs strongly, with no quantitative estimation of vertical turbulent dissipation rate (ϵ) or diffusivity coefficient (K_ρ). The estimation of K_ρ is very important for examining the formation of the water masses and further for the investigation of the thermohaline circulations in the Sea of Okhotsk and the North Pacific. Nakamura and Awaji (2004), using numerical tidal simulation, estimated the diapycnal diffusivity coefficient in the Kuril Straits. There have been several investigations to present a method for estimation of the vertical diffusivity from CTD data (e.g. Galbraith and Kelley, 1996). Specific estimation of ϵ and K_ρ will be shown in Chapter 3.

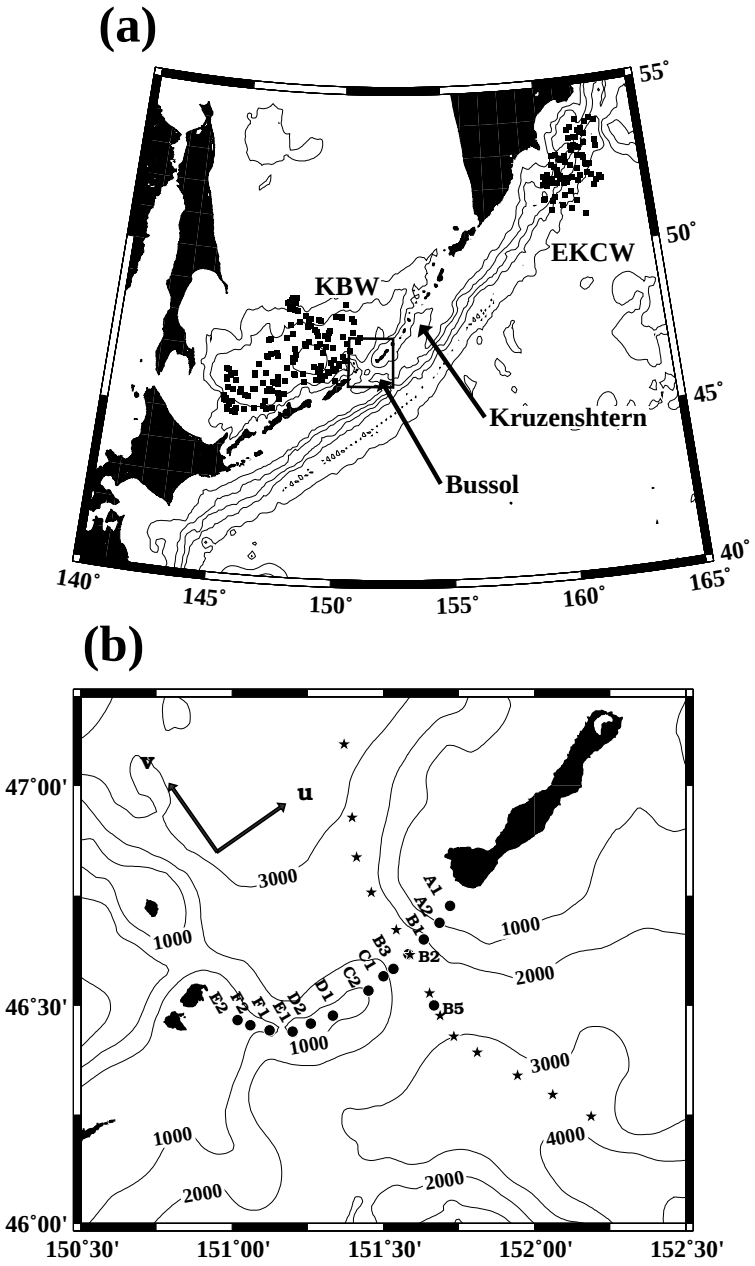


Figure 2.1 (a) Bathymetry around the Kuril Island Chain. Solid squares indicate stations data, which are used for the water mass analysis in Figs. 2.3 and 2.7. (b) Bathymetry in the vicinity of the Bussol′ Strait area within the rectangular box in (a) and the locations of the *XP01* stations. Solid circles indicate CTD stations and star symbols indicate XCTD stations. Bathymetry data are derived from the General Bathymetric Chart of the Oceans (GEBCO).

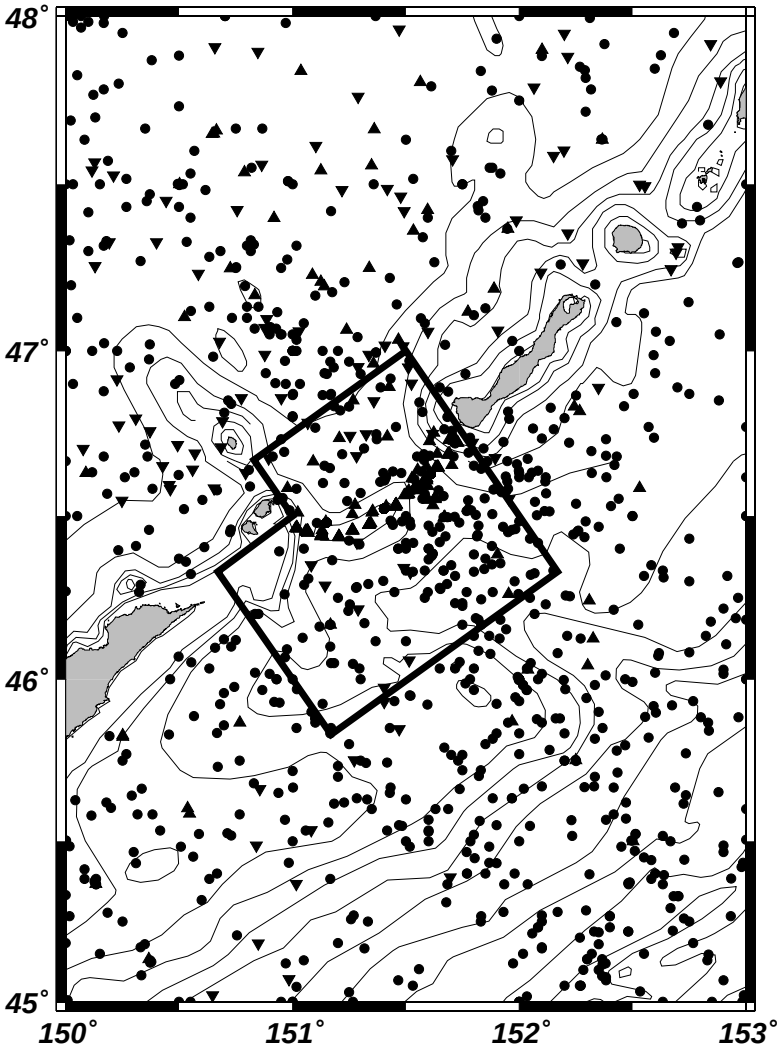


Figure 2.2 Distribution of all the available data at 26.8 σ_θ used in the present study. Circles, triangles, and inverted triangles indicate the online data (WOD01 and J-DOSS), data from recent specific cruises (*Prof. Khromov* from 1998 to 2001 and R/V *Kaiyo-Maru*), and profiling floats, respectively.

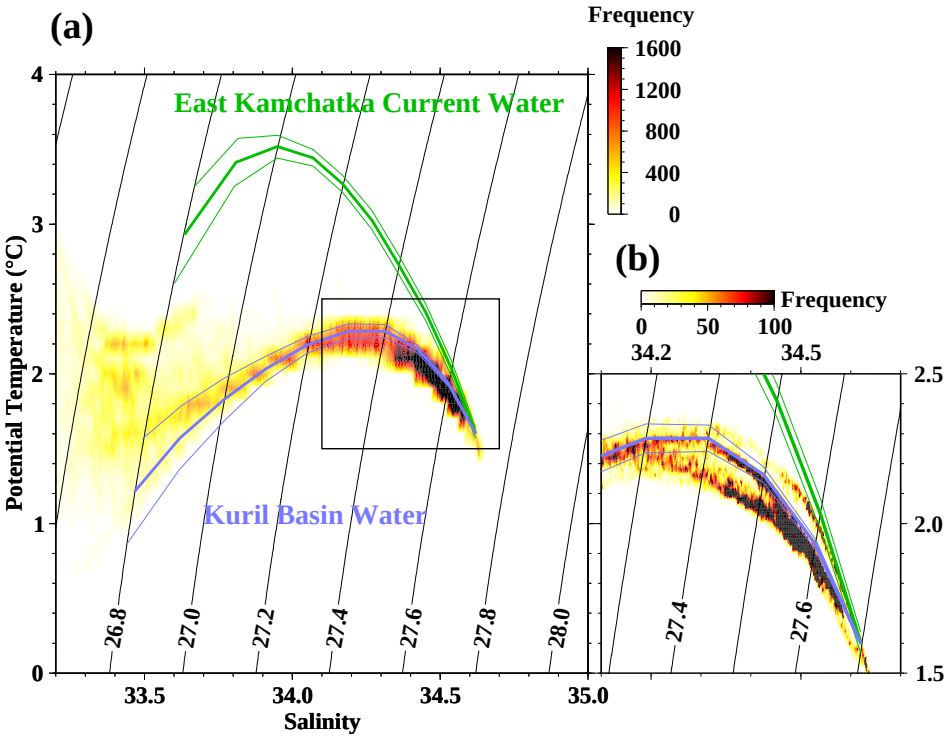


Figure 2.3 Distribution of the occurrence frequencies on the potential temperature-salinity diagram in the Bussol′ Strait calculated from all CTD data taken during *XP01*. (a) Frequency is counted on intervals of 0.1 °C in θ and of 0.01 psu in salinity. (b) Enlargement of rectangular box in (a). Frequency is counted on intervals of 0.02 °C in θ of 0.002 psu in salinity. Averaged profile of EKCW (green lines) and that of KBW (blue lines) are also shown with their standard deviation of potential temperature on potential density.

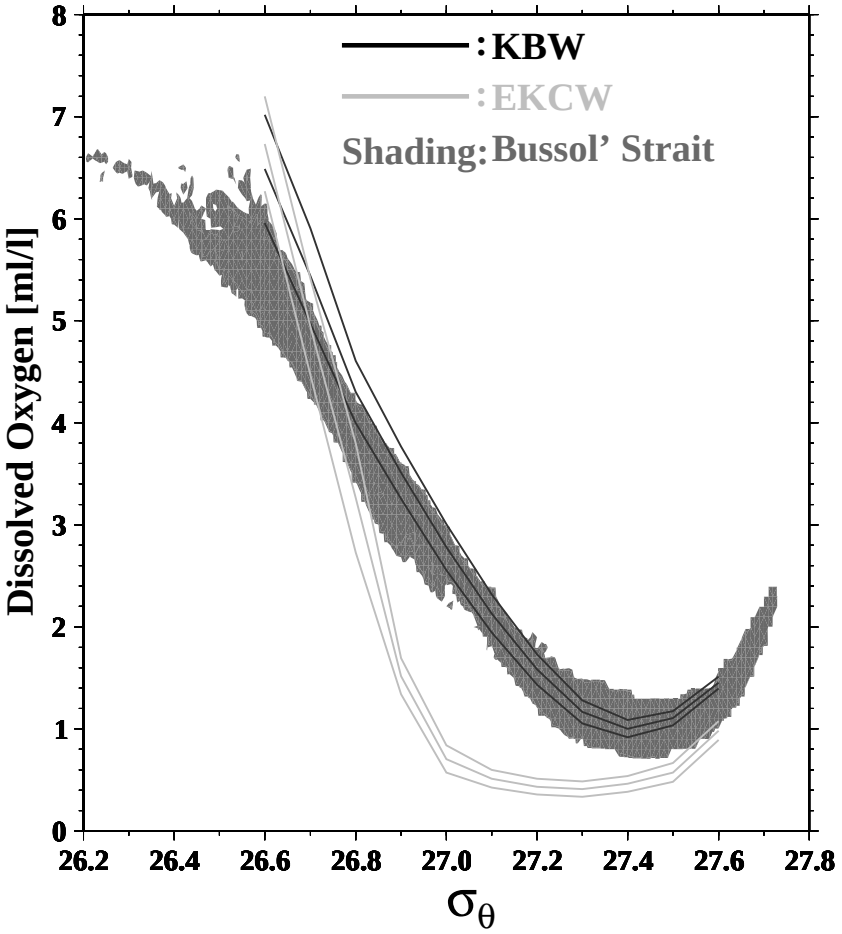


Figure 2.4 Distribution of the occurrence frequencies of the the dissolved oxygen content versus potential density in the Bussol′ Strait, from all CTD data taken during *XP01*. Frequency is counted on intervals of 0.01 in σ_θ and of 0.01 ml/l in dissolved oxygen content. Shading indicates frequencies higher than 40. Averaged profile of EKCW (gray lines) and that of KBW (black lines) are superimposed with their standard deviation. For calculation of the two water mass properties, we adopted 13 and 15 CTD station data for KBW and EKCW, respectively.

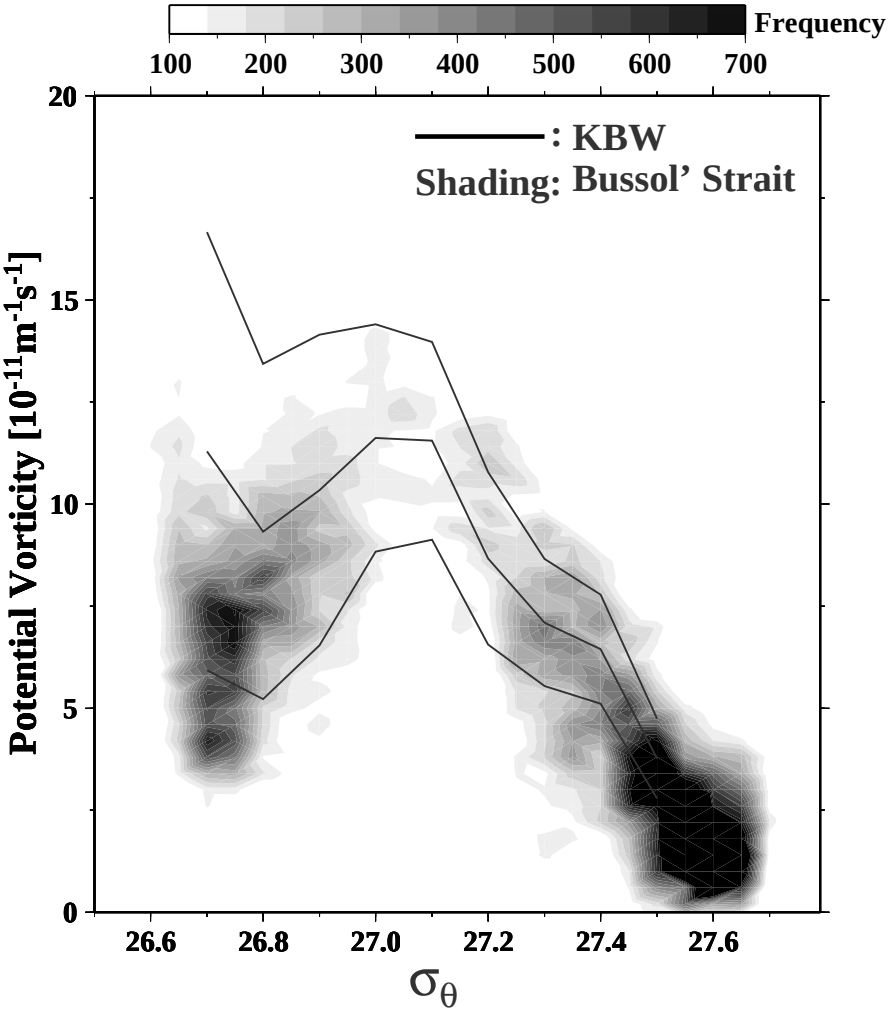


Figure 2.5 Distribution of the occurrence frequencies of the potential vorticity versus potential density in the Bussol′ Strait calculated from all CTD data taken during *XP01*. Frequency is counted on intervals of $0.4 \times 10^{-11}\,\mathrm{m^{-1}s^{-1}}$ in potential vorticity and of 0.05 σ_θ in potential density. Solid lines denote the averaged potential vorticity profile of KBW with the standard deviation from the profiling float and CTD data taken in the cruises of *Prof. Khromov* in 1998, 1999 and 2000.

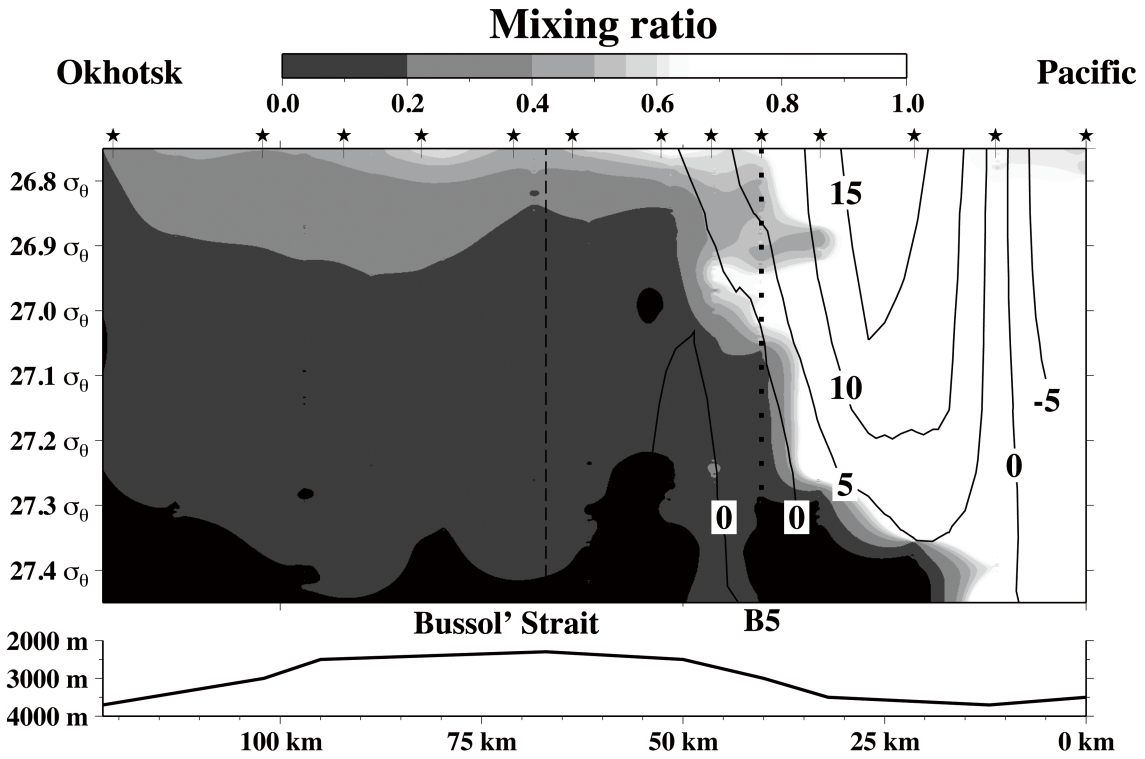


Figure 2.6 Mixing ratio of KBW to EKCW as a function of the potential density on the vertical section crossing the Bussol′ Strait from the Sea of Okhotsk to the Pacific, based on XCTD data of *XP01*. Star symbols indicate the XCTD stations. Water depth along the section is shown at the bottom. Broken line denotes the central position of the Bussol′ Strait. Position of Station B5 (see Fig. 2.1b for the location) is indicated by the dotted line. Geostrophic velocity relative to 1000 dbar is superimposed by the contour lines with positive values indicating southwestward flow.

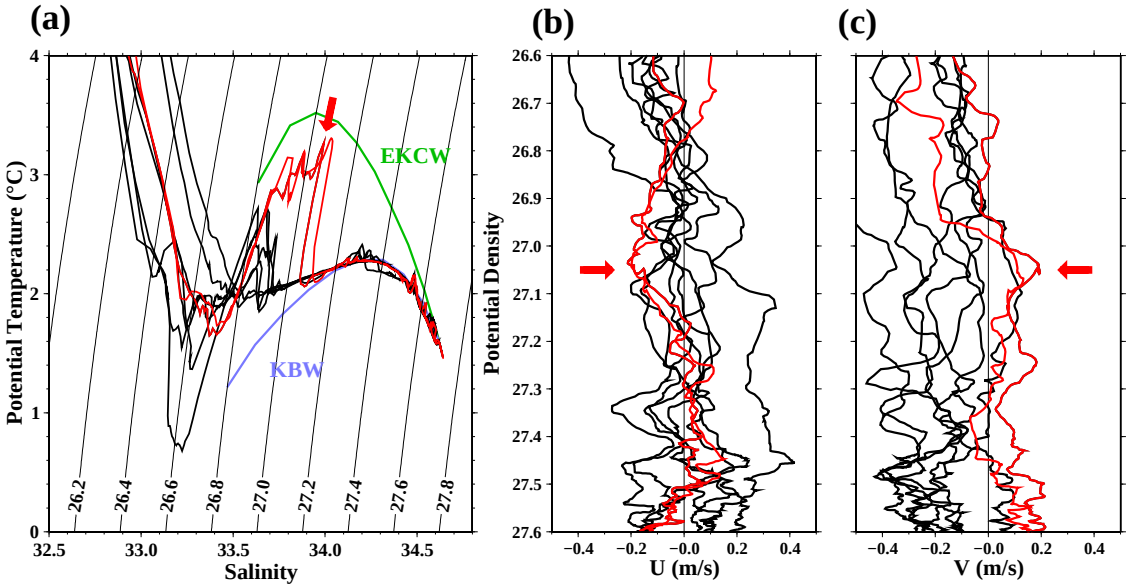


Figure 2.7 (a) Potential temperature-salinity diagram and vertical velocity profiles of the (b) northeast component and (c) northwest component as a function of the potential density from CTD and LADCP data taken at Station B5 (see Fig. 2.1b for the location). The two red curves in each panel indicate the casts in which the water mass property is most shifted to that of EKCW. Averaged profile of EKCW (green line) and of KBW (blue line) are shown in (a).

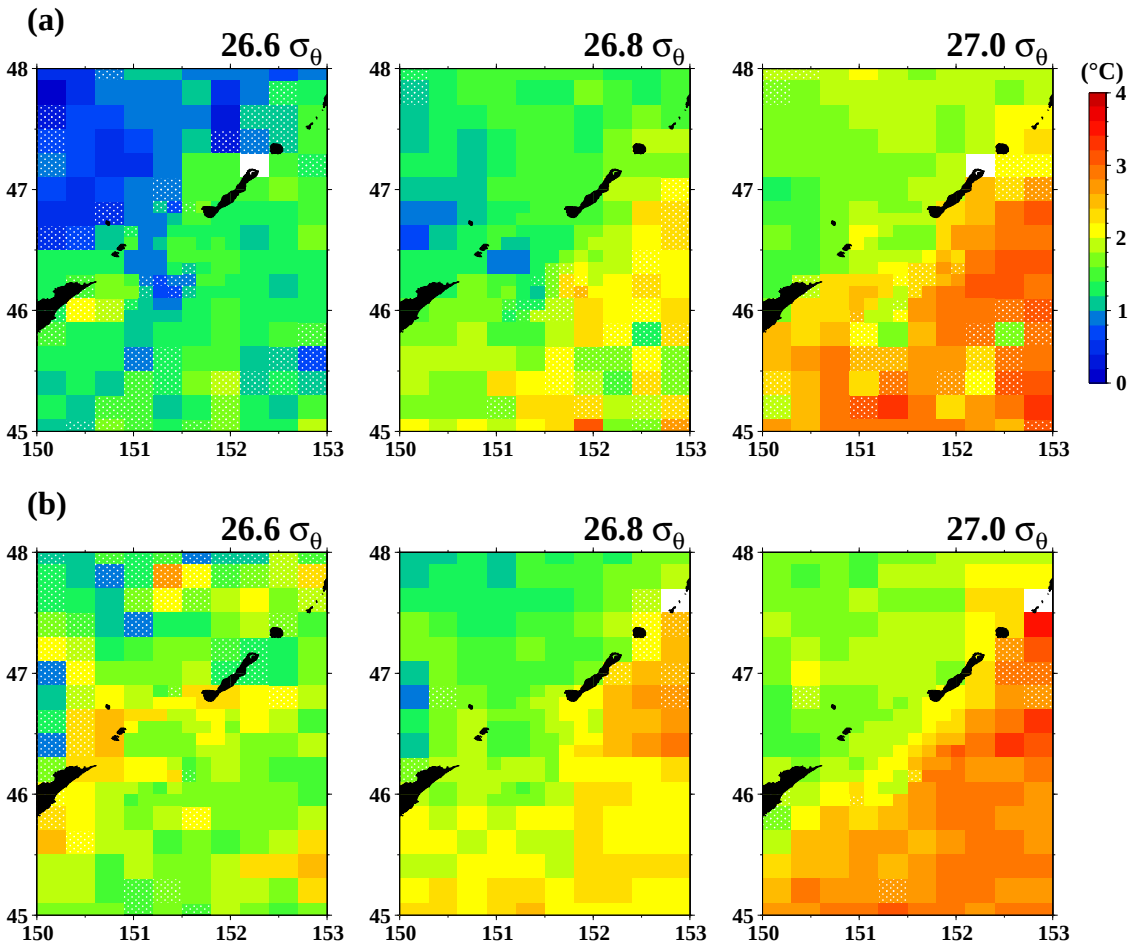


Figure 2.8 Horizontal distributions of potential temperature (°C) (a) from March to June (spring), and (b) from July to October (summer) on the 26.6, 26.8, and 27.0 σ_θ surfaces. A grid cell at which the standard error is more than 0.3 is shaded by white dots. At the 90% confidence level, the standard error is given by $1.645 \cdot \sigma/\sqrt{n}$, where σ is the standard deviation and n is the number of data. For grid cells with no data or fewer than three observations within the influence radius, that grid cell is regarded as a deficit and colored white.

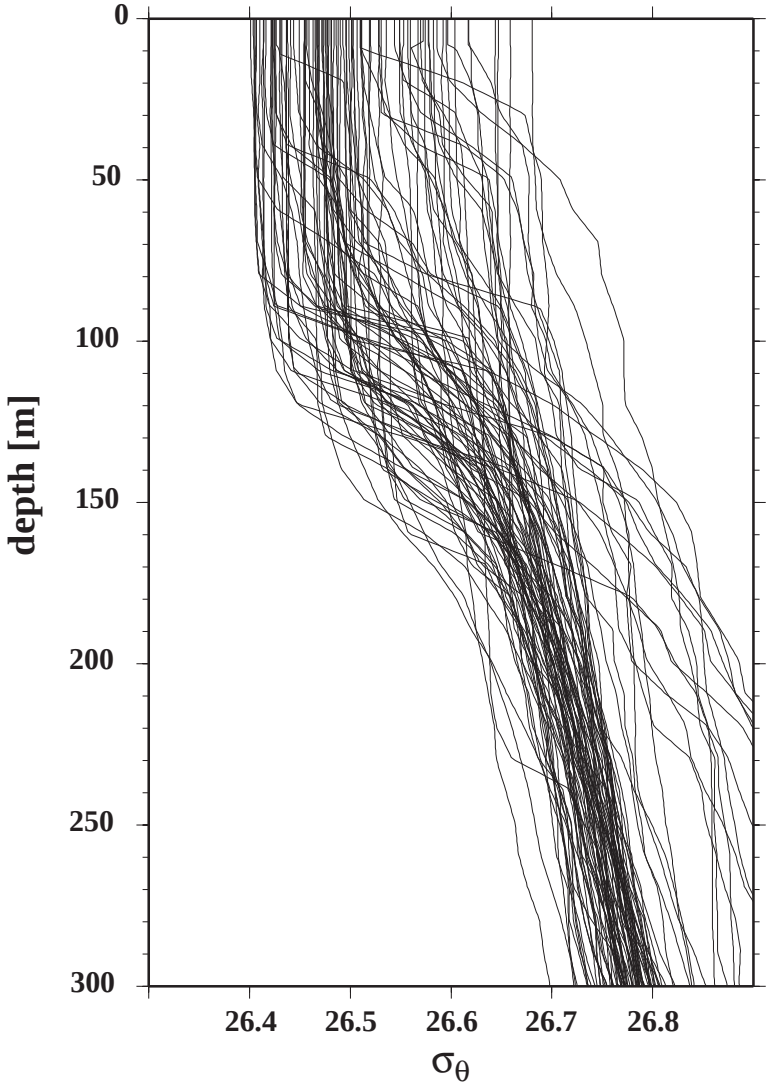


Figure 2.9 Potential density profile from all the available profiling floats from January to March in the Sea of Okhotsk and Pacific near the Bussol′ Strait.

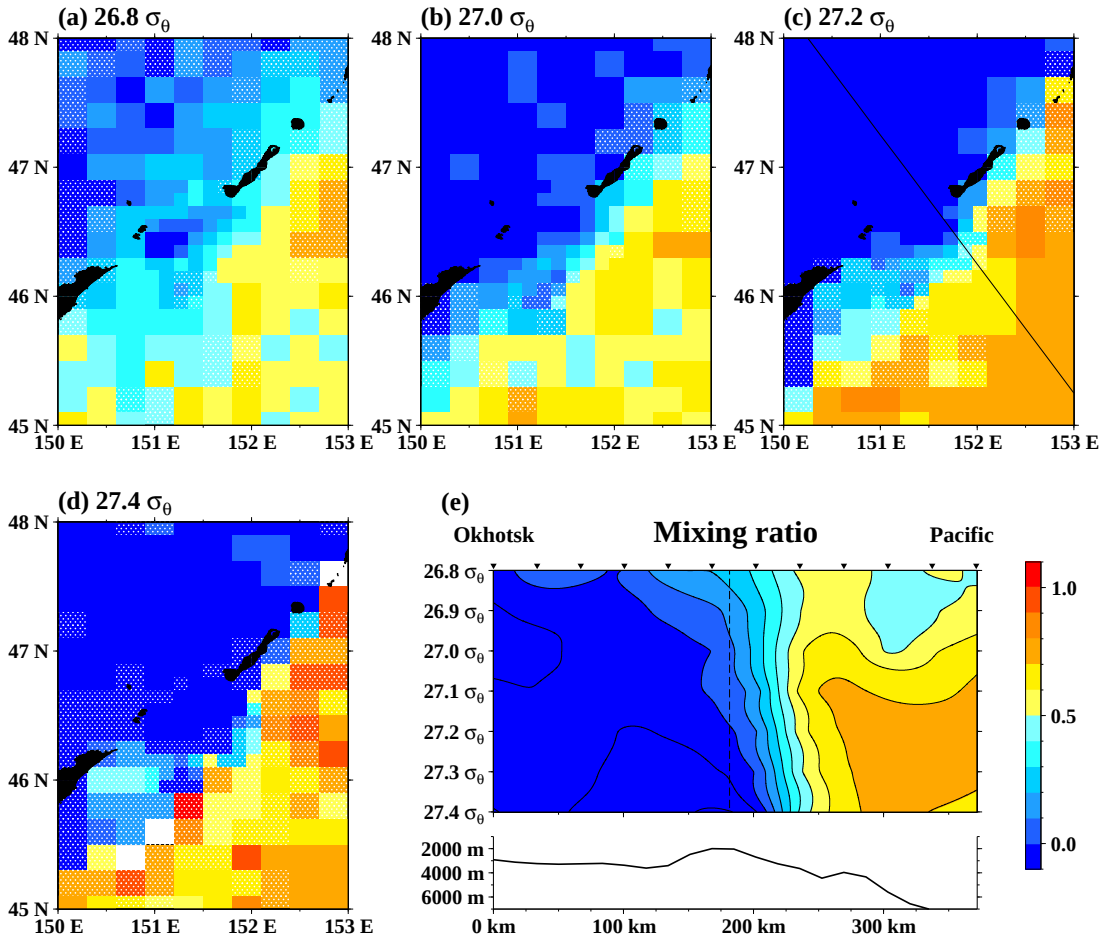


Figure 2.10 Horizontal distributions of mixing ratio of KBW to EKCW on (a) 26.8 σ_θ, (b) 27.0 σ_θ, (c) 27.2 σ_θ, and (d) 27.4 σ_θ surfaces. Warmer color indicates water closer to EKCW. A grid cell at which the standard error is more than 0.1 is shaded by white dots. Error estimate is the same as that of Fig. 2.8. Deficit grid cells are colored white. (e) Mixing ratio of KBW to EKCW on the vertical section designated in (c).

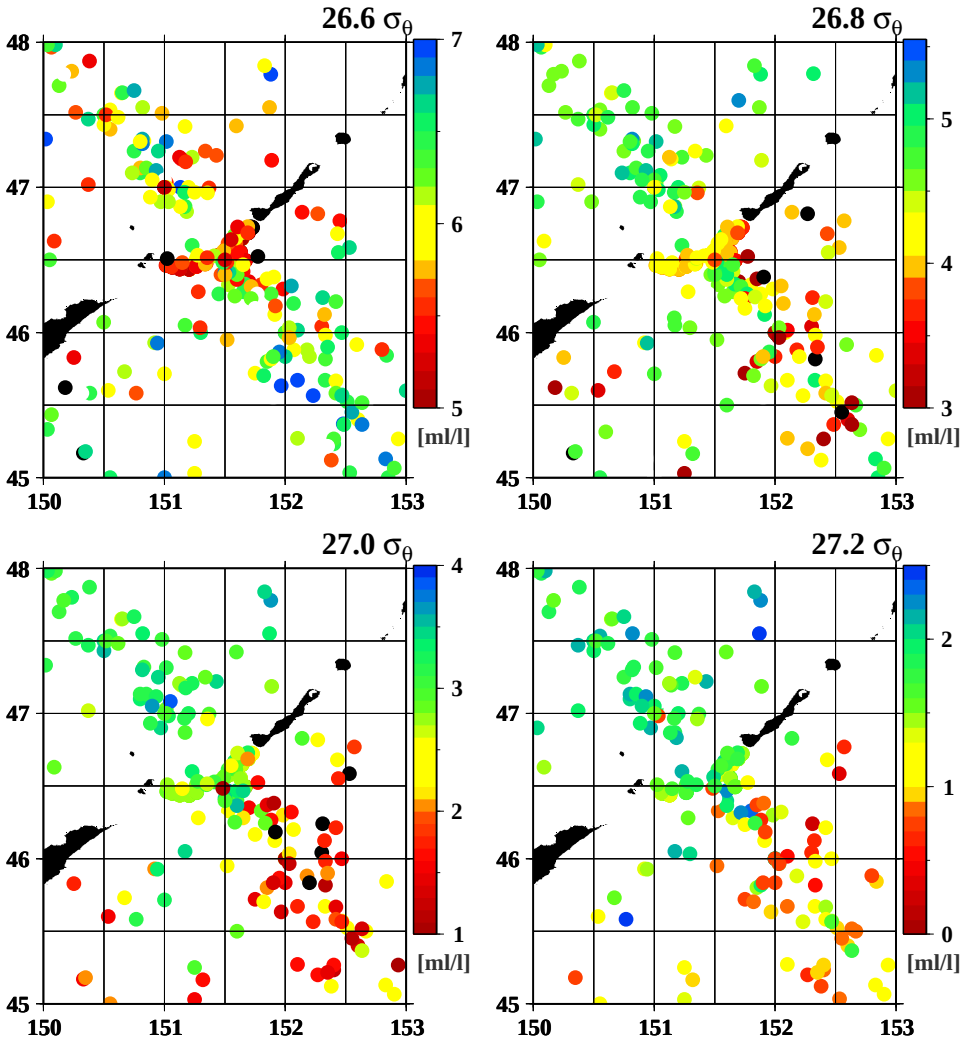


Figure 2.11 Plots of dissolved oxygen content on selected isopycnal surfaces, based on all available historical data.

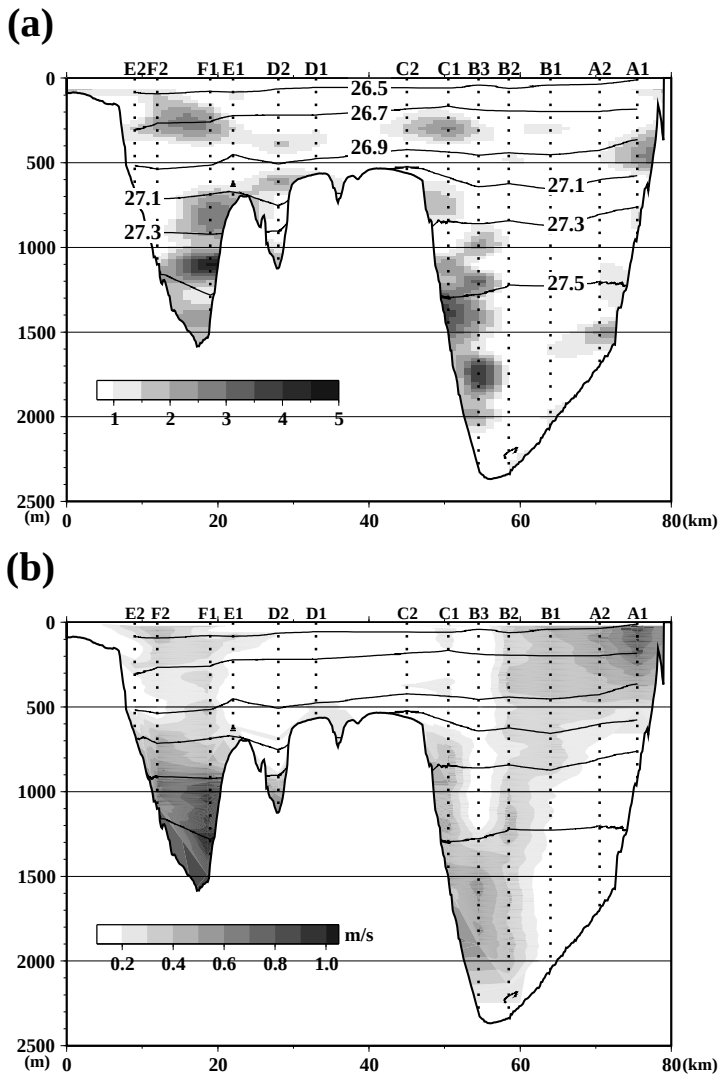


Figure 2.12 (a) Vertical section of the occurrence frequencies of the density inversion in the Bussol′ Strait. Frequencies are calculated from vertical density profiles of CTD data interpolated to 5 dbar intervals. First, we compute the vertical gradient by linear square fitting over a 20 m range with 5 data points. Negative values of the vertical density gradient are identified as density inversions. Then we count the number of density inversions for every 100 dbar, and average the number of density inversions from 12–18 casts for all 13 stations (A1, A2, B1, B2, B3, C1, C2, D1, D2, E1, F1, F2, and E2). We use the spring tide data for deep stations of the two channels, where the observations were made in both spring and neap tides. Isopycnals are shown by contours with the interval of $0.2\,\sigma_\theta$. (b) Amplitude of the diurnal tidal current measured with LADCP (from Katsumata *et al.*, 2004).

Chapter 3

Distribution of vertical diffusivity in the Bussol′ Strait: A mixing hot spot in the North Pacific

3.1 Introduction

The Sea of Okhotsk is the main site for ventilation of intermediate water in the North Pacific, including North Pacific Intermediate Water (NPIW) (Talley, 1991; Warner et al., 1996). Ventilation of NPIW is derived from sinking of surface water associated with high sea-ice production along the northern shelf region of the Sea of Okhotsk (Shcherbina et al., 2003) and strong tidal (vertical) mixing in the Kuril Straits. Based on chlorofluorocarbon (CFC) data, Wong et al. (1998) have suggested that strong vertical mixing in the Kuril Straits is the primary contributor to the ventilation in the density range of $> 27.1\,\sigma_\theta$. The Kuril Straits is also an important site for water mass transformation due to the strong tidal mixing. The water mass with a density of about $26.8\,\sigma_\theta$ has the largest thickness and thus the lowest potential vorticity in the Sea of Okhotsk (Yasuda, 1997; Itoh et al., 2003). In this density range, the Sea of Okhotsk is suggested as a possible source of the low potential vorticity of NPIW (Yasuda, 1997; Watanabe and Wakatsuchi, 1998), assuming a relatively small contribution of relative vorticity for large scale water mass distribution.

Several investigations have suggested that strong vertical mixing in the Kuril Straits has a substantial impact on the water mass distributions and thermohaline circulation

in the North Pacific. Based on the results of an analytical model, Tatebe and Yasuda (2004) pointed out that upward diapycnal transport from deeper layers due to vertical mixing in the Kuril Straits could be an important factor in determining the extent of the Oyashio and cross-gyre western boundary transport. Nakamura et al. (2006), using an ocean general circulation model, have suggested that strong tidal mixing in the Kuril Straits enhances the ventilation of the NPIW layer. Kawasaki and Hasumi (2010), on the basis of both a general circulation model and a box model, showed that the thermohaline circulation of the North Pacific depends strongly on the vertical profile of the vertical diffusivity coefficient K_ρ in the Kuril Straits. When strong vertical mixing reaches the sea surface, localized upwelling of deep water occurs, resulting in a single meridional circulation cell in the North Pacific. On the contrary, when strong mixing does not reach the surface, downwelling occurs in upper layers, whereas upwelling occurs in lower layers around the Kuril Straits, resulting in a double circulation structure in the North Pacific. Although the results of these numerical studies have not been confirmed by observations, they demonstrate the potential importance of vertical diffusivity in the Kuril Straits.

It is therefore vital to evaluate the strength and vertical structure of vertical diffusivity in the Kuril Straits. In recent years, several studies have estimated the magnitude of vertical mixing in the straits. Tanaka et al. (2007, 2010a) mapped the depth-averaged K_ρ values around the Kuril Straits, based on a physical model fitted by tidal elevation from TOPEX/POSEIDON altimeter data. They have shown that the areal average of depth-averaged K_ρ around the Kuril Straits is $25 \times 10^{-4}\,\mathrm{m^2\,s^{-1}}$, although K_ρ is amplified in several narrow to as much as $\sim 500 \times 10^{-4}\,\mathrm{m^2\,s^{-1}}$. They pointed out that the vertical diffusivity of $200 \times 10^{-4}\,\mathrm{m^2\,s^{-1}}$ given by Nakamura et al. (2006) is too large. Recent observational studies have used a microstructure profiler to try to measure vertical diffusivity directly in the Kuril Straits. Itoh et al. (2010, 2011) used a vertical microstructure profiler (VMP-2000) to estimate vertical diffusivity in the Urup Strait, which is located southwest of the Bussol′ Strait (see Fig. 3.1 for the location). Direct observations of turbulent mixing have also been made with a VMP-2000 profiler at one station in the Bussol′ Strait

in 2006 and 2007 (Yagi and Yasuda, 2012, hereafter YY12).

According to the mapping of K_ρ from the model (Nakamura and Awaji, 2004; Tanaka et al., 2010a), the region of enhanced K_ρ is widely distributed in and around the Bussol' Strait among the Kuril Straits. Ono et al. (2007) have suggested that, because of strong tidal mixing, the Bussol′ Strait is an important site of water mass transformation within the Kuril Straits. Furthermore, anticyclonic eddies have been frequently observed near the Bussol′ Strait (Bulatov et al., 1999; Ohshima et al., 2005), and they are likely caused by baroclinic instability associated with strong tidal mixing (Nakamura and Awaji, 2004; Ohshima et al., 2005). The Bussol′ Strait therefore can be regarded as one of the mixing hot spots in the North Pacific. Furthermore, the Bussol′ Strait is the deepest (sill depth of 2400 m) and widest (width of 80 km) strait of the Kuril Straits and thus is thought to be the main conduit for the exchange of water masses between the Sea of Okhotsk and the Pacific. In fact, most surface drifters (Ohshima et al., 2002) and profiling floats (target depth of 500–750 m; Ohshima et al., 2010) deployed in the Sea of Okhotsk flowed out into the North Pacific through the Bussol′ Strait during the winter.

Across the Bussol′ Strait at 13 stations, intensive observations were conducted aboard the Research Vessel *Prof. Khromov* in 2001 (hereafter *XP01*), using a Lowered Acoustic Doppler Current Profiler (LADCP) and Conductivity Temperature Depth (CTD) profiler. Katsumata et al. (2004) have revealed the mean, diurnal, and semi-diurnal exchange flow based on these LADCP observations, which were repeated over a 24-hour period across the strait. The net transport was from the Sea of Okhotsk to the Pacific with the net value being about 9 Sv ($1\,\mathrm{Sv} = 10^6\,\mathrm{m^3\,s^{-1}}$). The dominant diurnal tidal current reached an amplitude of $> 1.0\,\mathrm{m\,s^{-1}}$ in the western channel of the strait, even at depths greater than 1200 m. The amplification and dominance of the diurnal tidal current in the strait has also been demonstrated by surface drifters (Ohshima et al., 2002).

Ono et al. (2007), from *XP01* CTD data, found a unique water mass that is colder, less-saline, and has a higher dissolved oxygen concentration than Kuril Basin Water (KBW) and East Kamchatka Current Water (EKCW) in the density range 27.3–27.6 σ_θ. These

properties cannot be explained by isopycnal mixing between the two water masses. This suggests that these unique water properties are created by the vigorous vertical mixing across density surfaces in the strait. Generally, KBW shows the minimum value of potential vorticity around $26.8\,\sigma_\theta$. In the Bussol′ Strait this minimum value becomes further lower than that of KBW (Ono et al., 2007). This suggests a possibility of the formation of low potential vorticity water around $26.8\,\sigma_\theta$ in the Bussol' Strait.

Both the *XP01* and YY12 studies involved observations made in the Bussol′ Strait with repeated casts over 24-hour periods to resolve the mean and tidal components. The YY12 study used the VMP-2000 profiler to make direct observations of turbulence. However, the observations were made at a single station hence were not necessarily representative of the mean features of turbulence in the Bussol′ Strait. In contrast, the *XP01* study did not involve direct observations of turbulence, but conducted intensive CTD and LADCP observations at 13 stations (total of 127 casts) across the strait from the shelf slope to the deepest part of the sill. In this study we estimated the distribution of vertical mixing in the Bussol′ Strait based on the density inversions of all the CTD data taken by *XP01*, with the focus being on vertical structure. The observations were made during both the spring and neap tides at several stations during *XP01*. This enabled an evaluation of the characteristics of mixing over a fortnightly period, which assessment has not previously been made in the Kuril Straits. In addition, the repeated LADCP observations combined with the CTD casts provided data with which to examine the relationship between turbulent mixing and tidal currents in the strait. This examination helped to advance our understanding of the mechanism responsible for vertical mixing in the strait.

3.2 Data and methods

A total of 127 CTD casts were carried out in the Bussol′ Strait from 31 August 2001 to 12 September 2001 on board the R/V *Prof. Khromov* (see Fig. 3.1 for locations of the stations). More than five casts were made at each station (A–E), and those casts took place over a time period of more than 24 hours to resolve the mean and tidal components.

For the stations in the two deep channels (groups B and F; see the bottom contours in Figs. 3.1 and 3.5), the measurements were done during both the spring and neap tides. For the other stations, the measurements were done between the spring and neap tides. Details of the observational design are described in Katsumata et al. (2004).

We used the Seabird SBE-911 plus CTD system (Seabird, Bellevue, USA). Based on a post-cruise calibration and a comparison of water samples with a Guildline AUTOSAL salinometer, the accuracy of the CTD was 0.002 °C for temperature, 0.002 psu for salinity, 0.015% for depth, and thus 0.0016 $\mathrm{kg\,m^{-3}}$ for potential density. Raw CTD data were converted to 0.2 dbar intervals with a standard noise removal protocol (Ono et al., 2007). Only downcast data were used because the upcasts often stopped for bottle sampling, and the motion of the frame created turbulence around the CTD sensor.

There have been many studies to make quantitative estimations of vertical diffusivity from CTD data. These estimations have been based on the vertical length scale of overturns (e.g., Stansfield et al., 2001; Kitade et al., 2003; Thompson et al., 2007). The vertical length scale of overturns reflects the degree of water mass mixing activity. In this section, we briefly describe the concepts that we implemented in our study to estimate vertical turbulent diffusivity from the length scale of overturns.

The Ozmidov scale L_O (Ozmidov, 1965) is given by

$$\epsilon = L_\mathrm{O}^2 \cdot N^3, \tag{3.1}$$

where ϵ is the dissipation rate of turbulent kinetic energy defined as $\epsilon = (15/2)\cdot\nu\cdot(\partial u/\partial z)^2$, where ν is the molecular kinematic viscosity. The variable N is the buoyancy frequency defined by $\mathrm{N}^2 = -g/\rho \cdot \partial\rho/\partial z$, where g is the gravitational acceleration and ρ is the observed potential density. In terms of energy conversion, L_O corresponds to the vertical scale l within which scale all of the parcel's kinetic energy (proportional to the square of the vertical velocity w) is converted to potential energy (proportional to $N^2 \cdot l^2$) (Ferron et al., 1998). This implicitly assumes that $\epsilon \sim w^3/l$.

The Thorpe scale L_T (Thorpe, 1977) is a measure of the vertical scale of overturning.

Thorpe (1977) first proposed a way to extract the turbulence length scale from a potential temperature profile in the case of freshwater. He introduced the concept of ordering an observed temperature profile to obtain a gravitationally stable profile. The reordering is based on the idea that water parcels in a gravitationally stable profile have been displaced vertically by the turbulent motion. Following Thorpe's (1977) approach, here we derive the vertical displacement scale from a potential density profile. To estimate L_{T}, we adopted the method of Galbraith and Kelley (1996, hereafter GK96) to identify 'real' overturns. Data processing (methodology) is described in detail in Appendix A.

Estimates of the turbulent energy dissipation rate ϵ are derived from each overturning scale. The Thorpe scale is expected to be proportional to the Ozmidov scale (Dillon, 1982; Crawford, 1986; Ferron et al., 1998). Dillon (1982) pointed out that empirically L_{T} can be proportional to L_{O}, i.e., $L_{\mathrm{O}} = c \cdot L_{\mathrm{T}}$, where c is a constant. Previous studies have shown that the constant c ranges over 0.41–0.95 (Itsweire, 1984; Crawford, 1986; Ferron et al., 1998; Yagi and Yasuda, 2013). In this study, we adopted $c = 0.41$, based on the work of Yagi and Yasuda (2013), who derived a value $c = 0.41$ based on a comparison of CTD data with VMP-2000 data taken at several stations in the Bussol′ Strait. Equation (3.1) then reduces to

$$\epsilon_\rho \approx 0.168 \cdot {L_{\mathrm{T}}}^2 \cdot N^3 \ [\mathrm{W\ kg^{-1}}]. \tag{3.2}$$

Meanwhile, Osborn (1980) showed that the vertical diffusivity K_ρ is represented by $\mathrm{K}_\rho = \Gamma \cdot \epsilon / N^2$ where Γ is the mixing efficiency, which we assumed to be 0.2 (Osborn, 1980; Moum, 1996). Finally, vertical diffusivity K_ρ is given by

$$\mathrm{K}_\rho \approx 0.034 \cdot N \cdot {L_{\mathrm{T}}}^2. \tag{3.3}$$

We calculated the N based on the reordered potential density profile. In this study, Eqs. (3.2) and (3.3) were used for the estimation of the turbulent energy dissipation rate ϵ_ρ and the vertical diffusivity coefficient K_ρ, respectively. We note that YY12 used $c = 0.67$ based on the CTD/VMP observations at a single station. Use of $c = 0.67$

would cause the calculated values of K_ρ and ϵ_ρ to be 2.7 times the corresponding value obtained with $c = 0.41$.

To calculate the depth-averaged vertical diffusivity coefficient $\overline{K_\rho}$ and turbulent energy dissipation rate $\overline{\epsilon_\rho}$, we used the following averaging over the depth range H:

$$\overline{K_\rho} = \frac{\sum_{i=1}^{n} K_{\rho i} L_{zi}}{H}, \qquad \overline{\epsilon_\rho} = \frac{\sum_{i=1}^{n} \epsilon_{\rho i} L_{zi}}{H}, \tag{3.4}$$

where $K_{\rho i}$ and $\epsilon_{\rho i}$ are the vertical diffusivity coefficient and turbulent energy dissipation rate of the ith overturn, respectively; a total of n overturns exists in the depth range H and L_{zi} is the vertical scale of the ith overturn.

3.3 Results

Using Eqs. (3.2), (3.3), and (3.4), we calculate the Thorpe scale (L_T), K_ρ, and ϵ_ρ at 13 stations (total of 127 CTD casts) across the Bussol′ Strait, based on all the density inversions that passed by the run-length and water mass tests (Appendix A). Table 3.1 provides a summary of the performance of these quality tests and the maximum and depth-averaged L_T, K_ρ, and ϵ_ρ. Among all the density inversions, the largest Thorpe scale of 140 m is found during the spring tide at Station C1 (see Fig. 3.1 for the location), that is shown in the enlarged view in the left panel of Fig. 3.2a. In the depths of 1200–1550 m the significant displacement of > 250 m is observed, resulting in the vertical diffusivity coefficient K_ρ and the turbulent energy dissipation rate ϵ_ρ being $5900 \times 10^{-4}\,\mathrm{m^2\,s^{-1}}$ and $2600 \times 10^{-9}\,\mathrm{W\,kg^{-1}}$, respectively. Such a large value has never been observed in any other regions of the North Pacific.

We next focus on the stations observed at both the spring and neap tides (Station B1, B2, B3, F1, and F2). The values of K_ρ and ϵ_ρ were one order of magnitude larger at the spring than neap tide (Table 3.1). Because we found large differences at Stations F1 and F2, we have compared the Thorpe displacements at the spring and neap tides at those stations (Fig. 3.3). At the spring tide, large density inversions of > 10 m fre-

quently occurred with the largest displacement exceeding 200 m. The active inversions were confined from the bottom to 600 m above the bottom, with the exception of a large inversion around 600–800 m depths at 14:00 on September 1. In contrast, only a very few, small inversions occur from the surface to a depth of 500 m. At the neap tide (Fig. 3.3b), fewer and much smaller overturns occurred, with the largest one being ∼50 m (see also Table 3.1). Figure 3.4 shows vertical profiles of (a) K_ρ and (b) ϵ_ρ estimated from the Thorpe scale at Stations F1 and F2. Within each 200 m depth interval ($H = 200$ m), we used the bootstrap method (Appendix B) to estimate the median values (with error bars) from the $\overline{\epsilon_\rho}$ and $\overline{K_\rho}$ values on all the casts at F1 and F2. The largest values ($K_\rho \sim 300 \times 10^{-4}\,\mathrm{m^2\,s^{-1}}$, $\epsilon_\rho \sim 400 \times 10^{-9}\,\mathrm{W\,kg^{-1}}$) are found at a depth of 1200 m during the spring tide. For most of the depths, K_ρ and ϵ_ρ are one order of magnitude larger at the spring tide than the neap tide (see right panel of Figs. 3.4a and b). The vertical profile of K_ρ during the spring tide is similar to the analogous profile reported in the YY12 study at a station close to Station F1 (Fig. 1.8). We estimated the vertically averaged K_ρ and ϵ_ρ to be $170 \times 10^{-4}\,\mathrm{m^2\,s^{-1}}$ and $180 \times 10^{-9}\,\mathrm{W\,kg^{-1}}$, respectively (Table 3.1). These values are comparable to those reported in the YY12 study; the values of K_ρ (ϵ_ρ) are $100 \times 10^{-4}\,\mathrm{m^2\,s^{-1}}$ ($180 \times 10^{-9}\ \mathrm{W\,kg^{-1}}$) and $44 \times 10^{-4}\,\mathrm{m^2\,s^{-1}}$ ($110 \times 10^{-9}\,\mathrm{W\,kg^{-1}}$) in 2006 and 2007, respectively.

We next show the cross-strait mapping of K_ρ and ϵ_ρ in the Bussol′ Strait based on all the CTD data from 13 stations during the spring and neap tides (Figs. 3.5a–d). The mapping is based on the median values with error bars from the bootstrap method with 100-m bins. At stations where a single set of repeated casts was done between the spring and neap tides (Stations A1, A2, C1, D1, D2, E1, and E2), the results are mapped for both for the spring and neap tides. Using the bootstrap method, the uncertainty of Figs. 3.5a–d is also shown in Fig. B1 of Appendix B. Especially large values of K_ρ were distributed over the slope around a seamount located in the central part of the strait (Stations B3, C1, and F1) at the spring tide (Fig. 3.5a), with the largest value exceeding $100 \times 10^{-4}\,\mathrm{m^2\,s^{-1}}$. The distribution of ϵ_ρ was similar to that of K_ρ (Figs. 3.5c and 3.5d).

There is a good correspondence between these distributions and the distribution of the amplitude of the diurnal tidal current (Fig. 3.5e).

Figure 3.5 demonstrates that K_ρ and ϵ_ρ are closely related to the diurnal tidal current. The YY12 study relates vertical diffusivity with the vertical current shear. The current shear is considered to be larger with a stronger tidal current. For simplicity, we introduce here a empirical equation to predict K_ρ from the amplitude of the cross-strait diurnal current v (see Fig. 3.1 for the direction). Figure 3.6 shows a scatter plot of K_ρ versus the squared amplitude of the diurnal current (proportional to the tidal current energy) by the logarithmic scales. Assuming that the tidal currents do not necessarily determine vertical mixing under the condition of weak tidal currents, we fit a least squares line (thin line in Fig. 3.6) to the data associated with diurnal current amplitudes of > 0.2 m s^{-1}. That line corresponds to the following equation:

$$\log_{10}(K_\rho) = 1.61 \times \log_{10}(V_{amp}^2) - 1.88, \tag{3.5}$$

where V_{amp} is the amplitude of the diurnal current. There is some correlation between $\log_{10}(V_{amp}^2)$ and $\log_{10}(K_\rho)$, but the correlation coefficient (r) is only 0.50. K_ρ can not be accurately determined solely from the amplitude of the diurnal current. However, determination of the amplitude of the diurnal current is facilitated by high-resolution numerical modeling, and hence the value of V_{amp} is more easily obtained than that of K_ρ. We thus propose that the empirical Eq. (3.5) is a practical way to obtain a zeroth-order approximation of K_ρ over a wide area, possibly for the whole area of the Kuril Island Chain. In contrast with the diurnal current, the semi-diurnal current unlikely affects vertical mixing because of the weak amplitude and small correlation with K_ρ ($r = 0.20$). In contrast, there is a modest correlation between the strength of the mean current and K_ρ ($r = 0.46$). This may be related to enhanced vertical mixing caused by a combination of the mean flow and diurnal tidal current, as discussed in YY12.

We here focus on Station F1 where the direct observation of turbulence was performed at the nearby station in the YY12 study. They calculated the mean and diurnal exchange

flow across the strait from 24-hour repeated LADCP observations. The profiles of the mean current and diurnal amplitude were similar in 2006 and 2007: the mean flow was towards the Pacific in the upper layer of $< 800\,\mathrm{m}$, whereas the opposite flow occurred in the lower layer of $> 800\,\mathrm{m}$. The amplitude of the diurnal current was amplified toward the bottom and reached $\sim 1.5\,\mathrm{m\,s^{-1}}$ at depths below 1000 m, which structure is explained by the first mode topographically trapped waves (TTW; Tanaka et al., 2010b). YY12 have speculated that the large vertical shear caused by a combination of the mean and diurnal currents within the depth range 800–1000 m causes the observed maximum of ϵ_ρ and K_ρ in this depth range. Also in our observation of *XP01*, the large vertical shear by their combination is found at the depth around 800 m (red line in Fig. 3.5f) and the large K_ρ occurs around 800 m depth (Fig. 3.4a). This co-occurrence suggests that the same mechanism causes strong vertical mixing at this depth.

The largest ϵ_ρ of $4700 \times 10^{-9}\,\mathrm{W\,kg^{-1}}$ is found at Station A1 (Table 3.1), that is shown in the enlarged view in the left panel of Fig. 3.2b. Because the amplitude of the diurnal tidal current is strong at this station (Katsumata et al., 2004), large water mass exchange occurs between the Sea of Okhotsk and the Pacific. Despite the observations were taken within a day, a significant different of the water mass property is found between the Sea of Okhotsk and the Pacific in the density range of $\sim 26.9\sigma_\theta$ (Fig. 3.7). In addition, since Station A1 is located over a steeply sloped bottom, the amplitude of the first mode TTW becomes large there (Tanaka et al., 2010b). The fact that the maximum ϵ_ρ is also found around $26.9\,\sigma_\theta$ at Station A1 (Fig. 3.5c) suggests that the large ϵ_ρ at this layer creates the low potential vorticity water that affects the NPIW formation.

Assuming that the results from the 13 stations across the Bussol′ Strait are representative of the vertical mixing in and around the strait, we have shown in Fig. 3.8 the raw and averaged profiles (based on all the CTD casts) of estimated K_ρ and ϵ_ρ values as a function of potential density, depth, and height from the bottom. We used a bootstrap technique to calculate median values of K_ρ (red lines) and ϵ_ρ (blue lines). Overall the profiles of K_ρ and ϵ_ρ are similar, whereas K_ρ shows relatively large values when compared

to ϵ_ρ at depths of $>1600\,\mathrm{m}$ (density range of $>27.6\,\sigma_\theta$) because of the small N^2. Around the density range of $27.6\,\sigma_\theta$ and depths of 1400–1600 m K_ρ shows the maximum value, reaching $\mathrm{K}_\rho > 100 \times 10^{-4}\,\mathrm{m^2\,s^{-1}}$, which is two to three orders of magnitude larger than the background diffusivity.

3.4 Discussion

Relatively large values of K_ρ (on the order of $10 \times 10^{-4}\,\mathrm{m^2\,s^{-1}}$) were estimated in the density range 27.5–$27.6\,\sigma_\theta$ (Fig. 3.8a). Here we discuss the relationship between strong vertical mixing and water mass transformation in this density range. Figure 3.9 shows a plot of potential temperature versus salinity for the cases of (a) large K_ρ ($> 60 \times 10^{-4}\,\mathrm{m^2\,s^{-1}}$) and (b) relatively small K_ρ ($< 10 \times 10^{-4}\,\mathrm{m^2\,s^{-1}}$) from all the CTD data taken during *XP01* in the Bussol′ Strait. In this plot, we find the colder and less-saline water which cannot be explained by isopycnal mixing between KBW and EKCW. This water can be explained by diapycnal mixing between adjacent layers (Ono et al., 2007). In the case of $\mathrm{K}_\rho > 60 \times 10^{-4}\,\mathrm{m^2\,s^{-1}}$ (Fig. 3.9a), almost all of the water is of this unique water mass (not of KBW and EKCW). While for $\mathrm{K}_\rho < 10 \times 10^{-4}\,\mathrm{m^2\,s^{-1}}$ (Fig. 3.9b), water with KBW or EKCW properties exists in addition to the unique water.

Figure 3.9 shows the potential temperature-salinity plot for the case at (c) spring and (d) neap tide. Although the unique water (colder and less-saline) mass occurs at both the spring and neap tide in the density range of 27.1–$27.6\,\sigma_\theta$, the occurrence frequency of $\mathrm{K}_\rho > 60 \times 10^{-4}\,\mathrm{m^2\,s^{-1}}$ was far more frequent during the spring tide (22%) than during neap tide (2%) (Fig. 3.9c). Here we defined unique water to be water with a potential temperature one standard deviation lower than that of KBW at a given σ_θ. Figure 3.10 shows the distribution of this unique colder and less-saline water across the Bussol′ Strait during the spring tide (stippled areas). The unique water is distributed over the slope of the central seamount of the strait, where intense vertical mixing occurs (Figs. 3.5a–d). These features suggest that the unique water is created locally in the strait by intense vertical mixing during spring tides, with the typical K_ρ of $> 60 \times 10^{-4}\,\mathrm{m^2\,s^{-1}}$ over the

slope of the central seamount of the strait.

Kawasaki and Hasumi (2010) suggested that the North Pacific thermohaline circulation is strongly influenced by the structure of vertical mixing in and around the Kuril Straits. Whether the strong vertical mixing in the straits reaches the sea surface or not, results in a single cell or double cells of the North Pacific thermohaline circulation. The present study suggests that K_ρ reaches a maximum on the order of $100 \times 10^{-4}\,m^2\,s^{-1}$ at depths of ∼1100–1700 m and a minimum on the order of $1.0 \times 10^{-4}\,m^2\,s^{-1}$ from the surface to 300 m (Fig. 3.8b). The implication is that strong vertical mixing does not reach the sea surface. If the vertical mixing in the Bussol′ Strait is representative of the mixing in the Kuril Straits, localized downwelling of surface water would be induced around the Kuril Straits, resulting in a double-celled thermohaline circulation in the North Pacific, according to Kawasaki and Hasumi (2010).

The vertical average of K_ρ calculated from the medians of all the depth intervals (Fig. 3.8b) is $60 \times 10^{-4}\,m^2\,s^{-1}$. This value is comparable to the areal mean of vertically averaged K_ρ values of $\sim 25 \times 10^{-4}\,m^2\,s^{-1}$ obtained by Tanaka et al. (2010a) from their numerical model. This value is one order of magnitude smaller than the K_ρ used by Nakamura et al. (2006). Figure 3.8c shows K_ρ (red line) and ϵ_ρ (blue line) in the Bussol′ Strait as a function of height from the bottom. Very strong vertical mixing on the order of $100 \times 10^{-4}\,m^2\,s^{-1}$ is observed from the bottom to a height of 400 m above the bottom. This likely results from the amplification of the diurnal tidal current near the bottom by the excitation of a diurnal topographic Rossby wave (YY12; Tanaka et al., 2010b). However, the maximum of K_ρ occurs around 300 m from the bottom unlike the topographic Rossby wave having the maximum amplitude near the bottom. This difference does not necessarily imply that turbulent mixing is damped near the bottom. Rather, there is a possibility that our indirect estimation could not adequately evaluate the turbulent mixing near the bottom, because the strong turbulence near the bottom may result in uniform density.

Finally, it should be noted that K_ρ and ϵ_ρ differed by almost one order of magnitude

during the spring and neap tides. This difference suggests that vertical mixing varies considerably during the fortnightly tidal cycle in and around the Kuril Straits. This variation might further induce the phenomena and circulation with a fortnightly cycle (e.g., Hibiya et al., 1998). For evaluation of the vertical mixing, the timing of in-situ observations (spring or neap tide) should be carefully considered, because the tidal cycle will affect the strength of the mixing. Previous numerical modeling studies (e.g., Nakamura and Awaji, 2004; Tanaka et al., 2010a) treated only the K_1 tide in their evaluation of vertical mixing in the Kuril Straits. Also in the numerical models, inclusion of the O_1 tide and thus the fortnightly cycle will be required for better evaluation of vertical mixing.

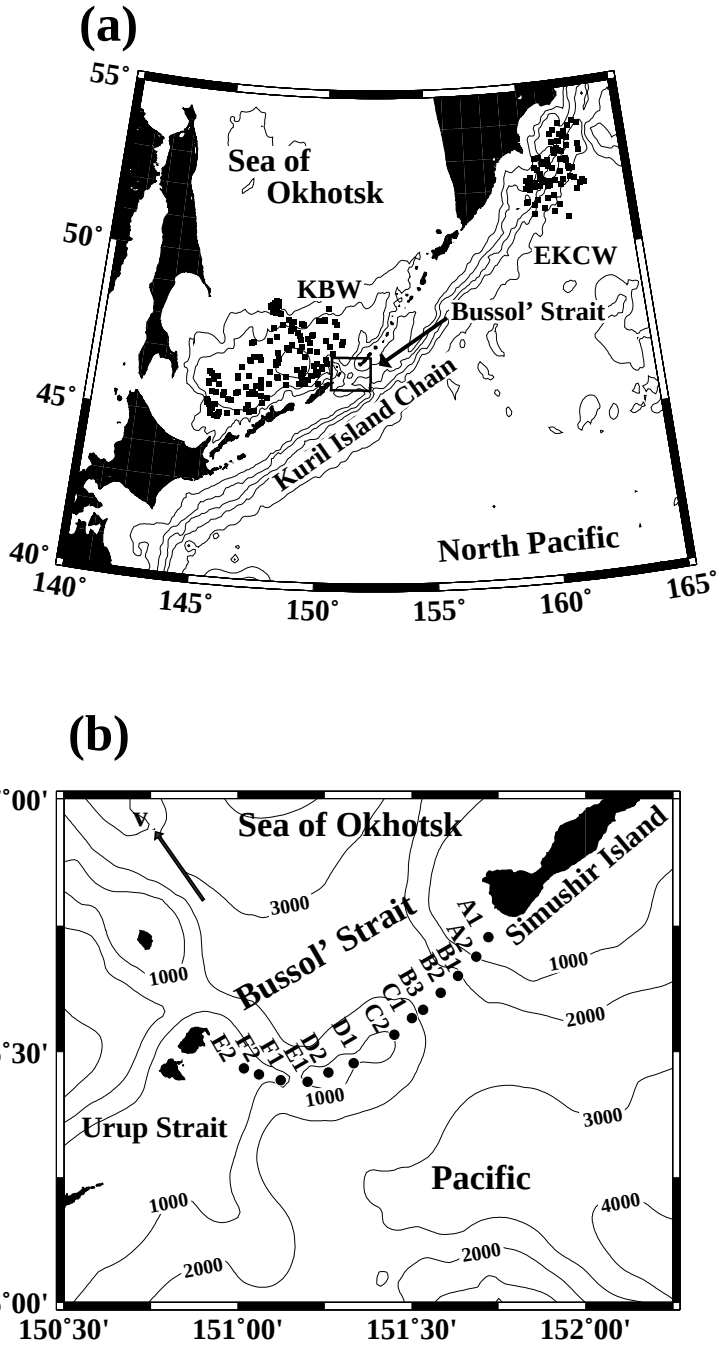


Figure 3.1 (a) Bathmetric map of the Sea of Okhotsk and the Kuril Island Chain. Solid squares indicate the stations used for calculating the mean properties of East Kamchatka Current Water (EKCW) and Kuril Basin Water (KBW) in Fig 3.9. (b) Enlarged map of the Bussol′ Strait area designated by the rectangular box in (a), with the *XP01* cruise CTD stations (solid circles). The bathymetric data are derived from the General Bathymetric Chart of the Oceans (GEBCO).

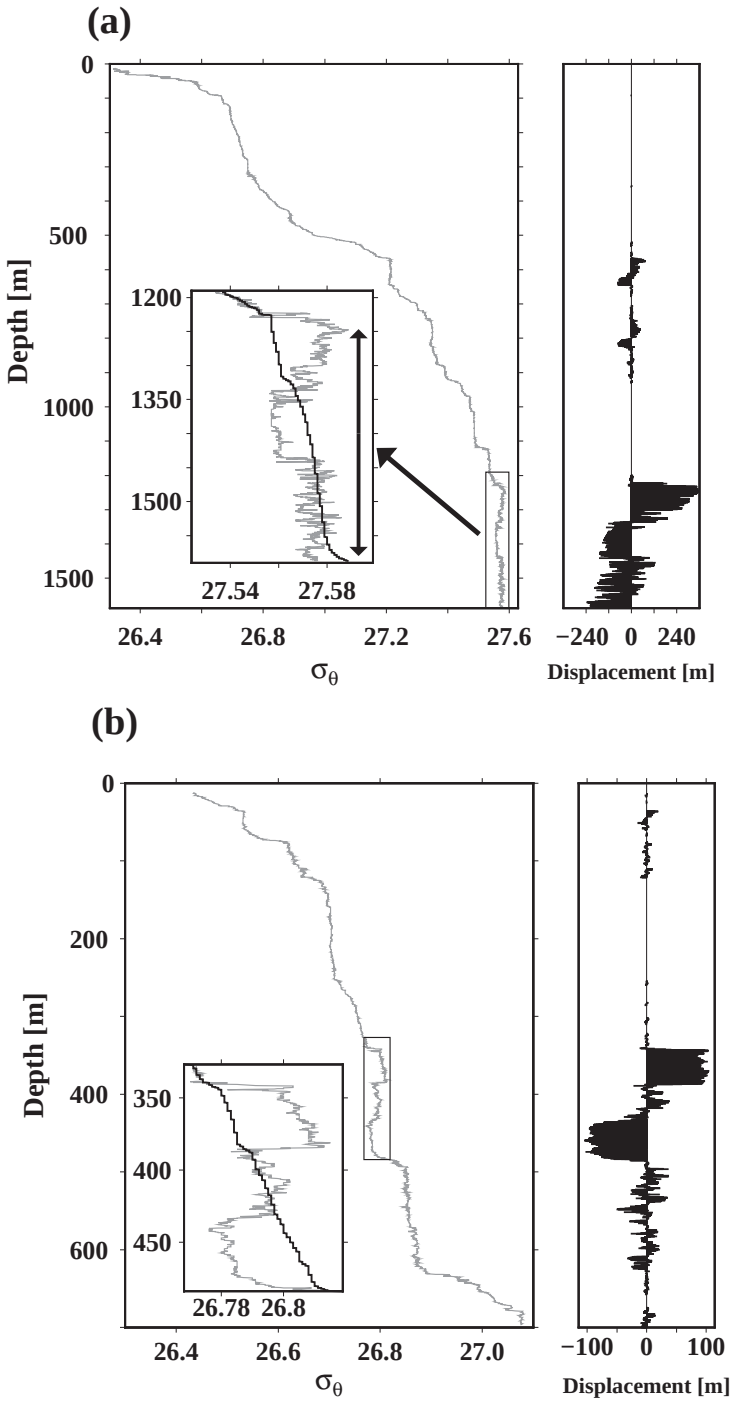


Figure 3.2 (a) Potential density and Thorpe displacement from the CTD data at Station C1 (see Fig. 3.1 for the location) at 3:00 on September 3. The layer of the maximum Thorpe displacement during *XP01* is indicated by the two-headed arrow. The left panel shows the vertical profile of the potential density with the enlarged profile (gray line) for the rectangular box and the profile reordered in gravitationally stable density (black line). The profile of Thorpe displacement after the run-length and water mass tests is shown in the right panel. (b) Same as (a), but for Station A1 at 14:00 on September 4.

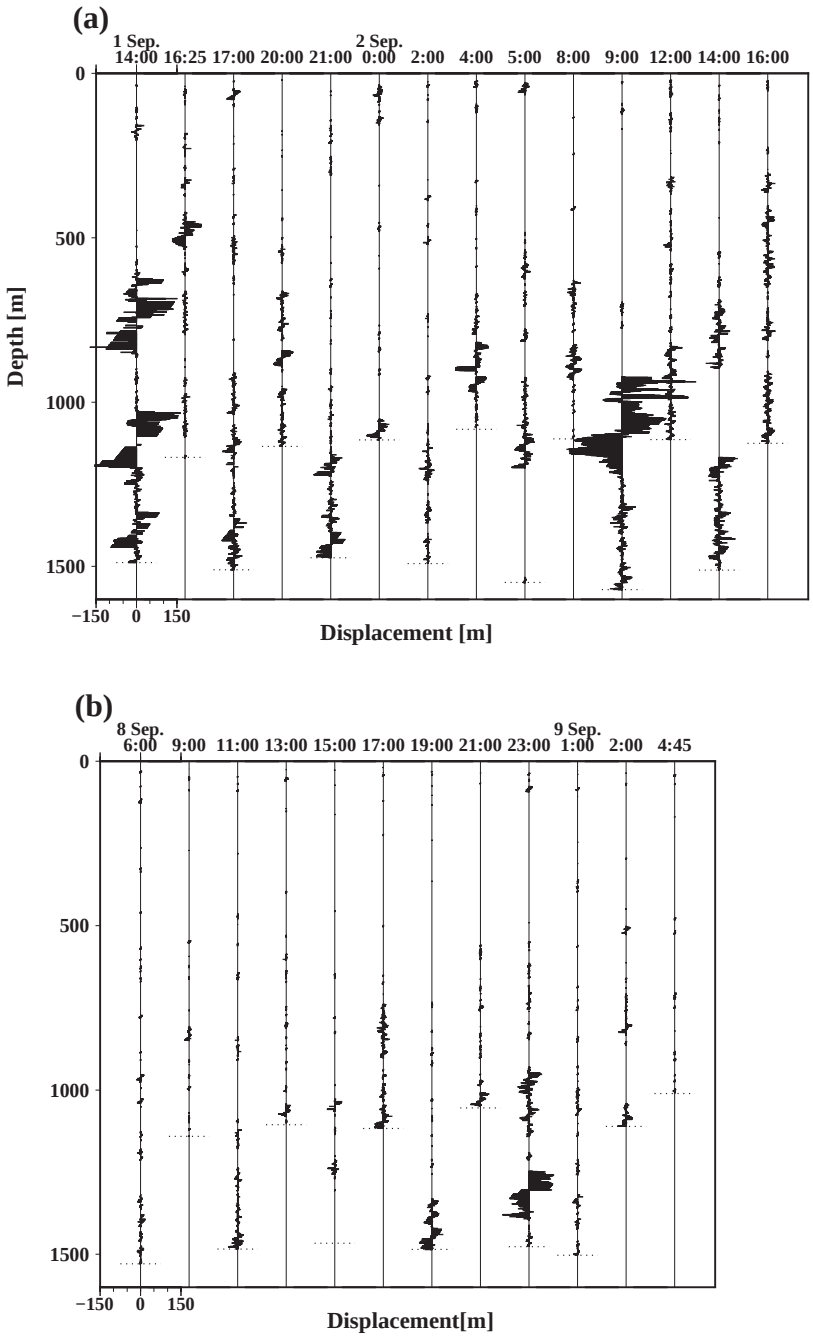


Figure 3.3 Vertical profiles of Thorpe displacements after the run-length and water mass tests at Stations F1 and F2 during (a) spring and (b) neap tides. The deployment time at each cast is drawn at the top. The bottom depth of each cast is indicated by a dotted line.

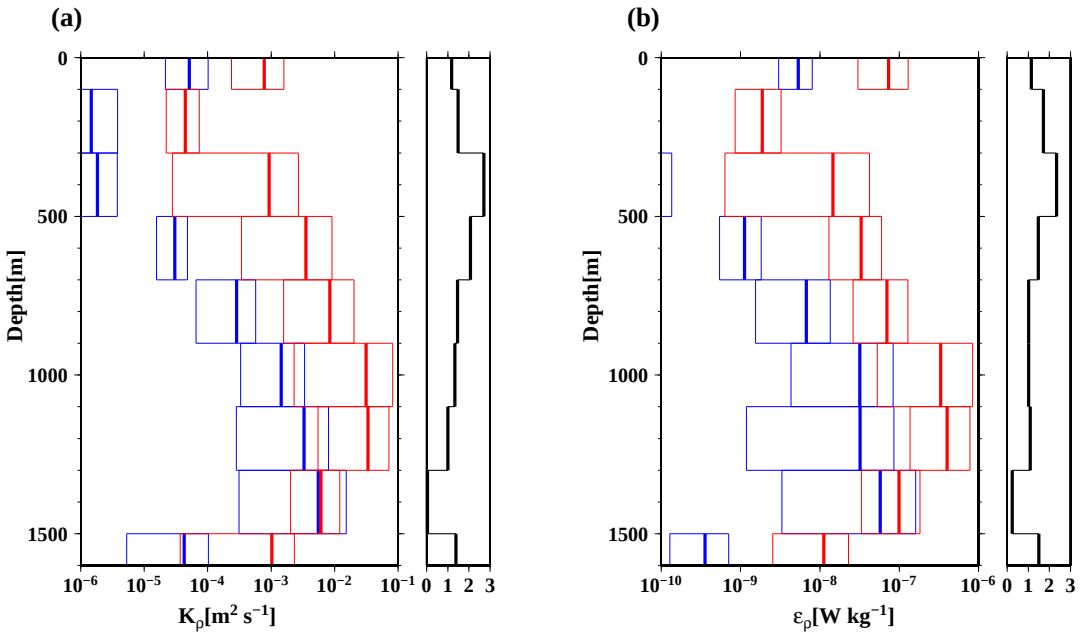


Figure 3.4 Average profiles of (a) K_ρ and (b) ϵ_ρ at spring (red lines from 14 casts) and neap (blue lines from 13 casts) tides every 200 m at Stations F1 and F2 (see Fig. 3.1 for the locations). Bold lines indicate the median value with the 95% confidence range denoted by thin lines, determined from a bootstrap method (Appendix B). The right-panel in (a) and (b) shows the ratio of the values at the spring and neap tides on a common logarithmic scale.

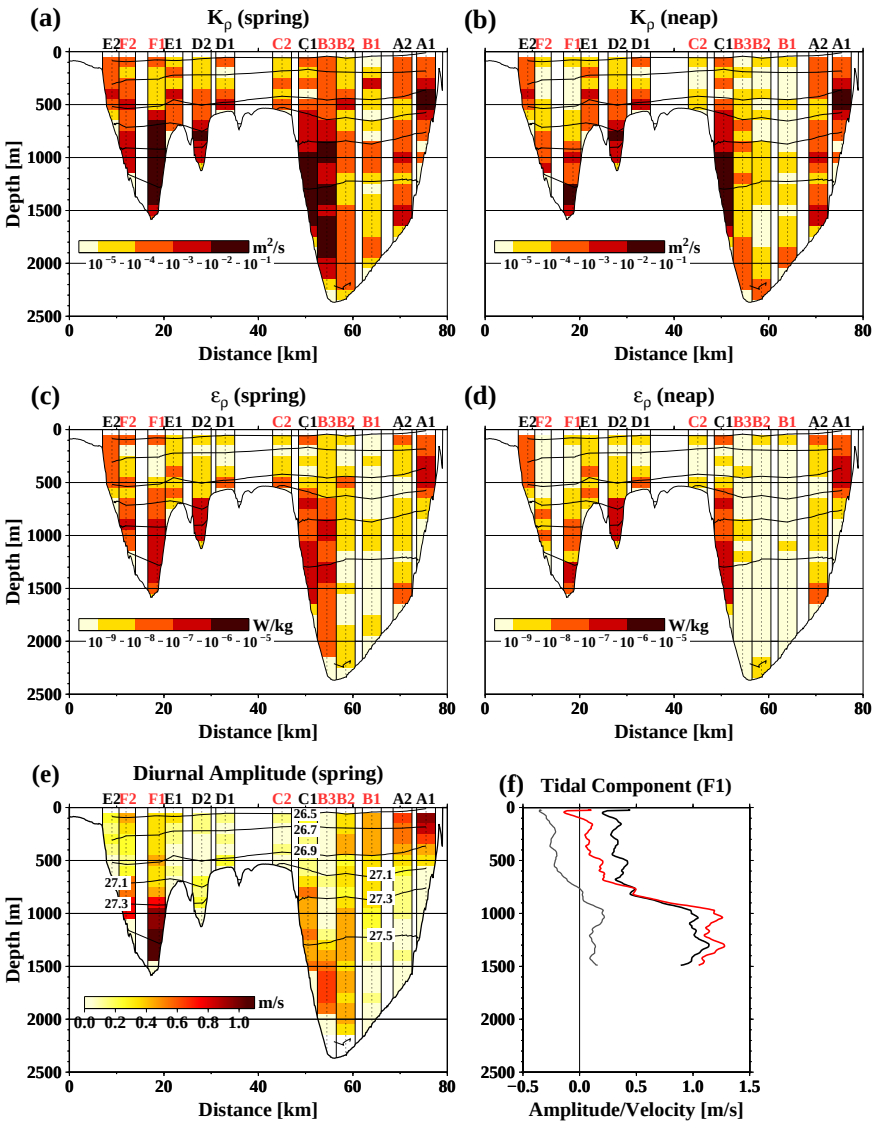


Figure 3.5 Cross-strait mapping of K_ρ and ϵ_ρ: (a) K_ρ at spring tide, (b) K_ρ at neap tide, (c) ϵ_ρ at spring tide, and (d) ϵ_ρ at neap tide. The values of K_ρ and ϵ_ρ at depth intervals of 100 m are determined by medians using a bootstrap method from 6–8 CTD casts at each station. The stations observed at both spring and neap tides are drawn in red characters (B1, B2, B3, C2, F1, and F2), and those observed at repeated casts on only one occasion between the spring and neap tides are drawn in black characters (A1, A2, C1, D1, D2, E1, and E2). (e) Amplitude of the diurnal tidal current measured with LADCP (from Katsumata et al. (2004)). In (a)–(e), the isopycnals are shown by contours at intervals of $0.2\,\sigma_\theta$. (f) Vertical profiles at Station F1 of the mean velocity (gray line), with positive indicating flow toward the Sea of Okhotsk, and of the diurnal current amplitude (black line). The red line indicates the sum of the mean and tidal currents when the diurnal tidal current toward the Sea of Okhotsk was maximum. This station is very close to the station observed by YY12.

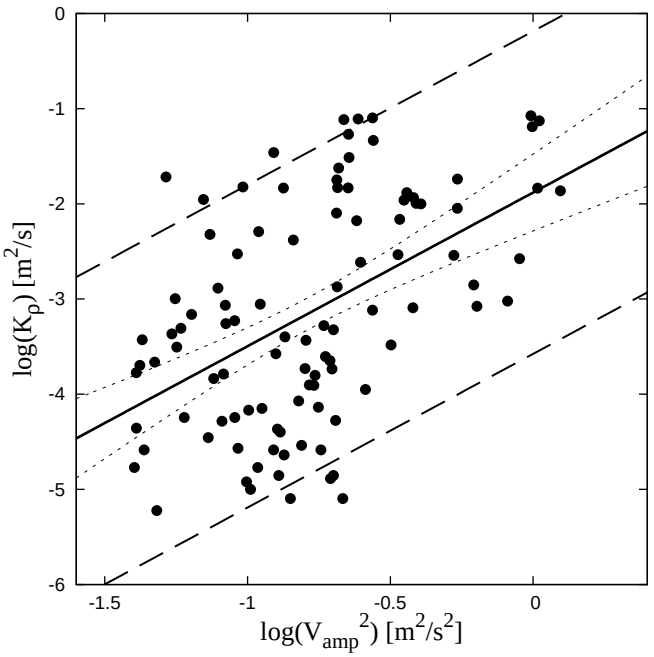


Figure 3.6 Scatter plots of K_ρ versus the squared amplitude of the across-strait diurnal current for current amplitudes of > 0.2 m s^{-1}. The plotting scale is logarithmic on both axes. The thick line is the regression fit, represented by $\log_{10}(K_\rho) = 1.61 \times \log_{10}(V_{amp}^2) - 1.88$, with the 95% confidence interval indicated by dotted lines. Dashed lines indicate the 90% prediction interval for the $\log_{10}(K_\rho)$ distribution, represented by $\log_{10}(K_\rho) = 1.61 \times \log_{10}(V_{amp}^2) - 1.88 \pm 1.66 \times S_e$, where S_e is the standard error.

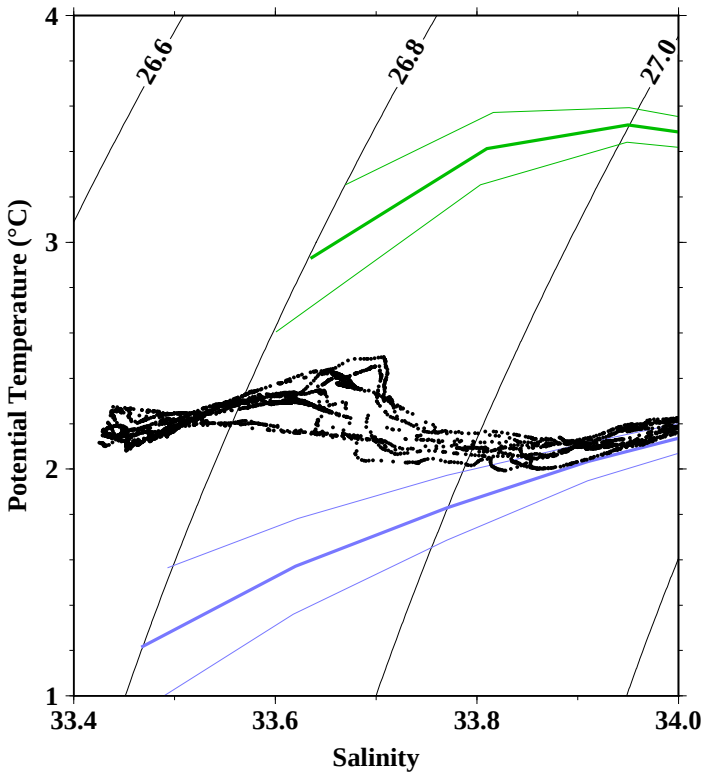


Figure 3.7 Potential temperature-salinity diagram from CTD data taken at Station A1 (see Fig. 3.1 for the location). Averaged profile of EKCW (green lines) and that of KBW (blue lines) are also shown with their standard deviation of potential temperature on potential density.

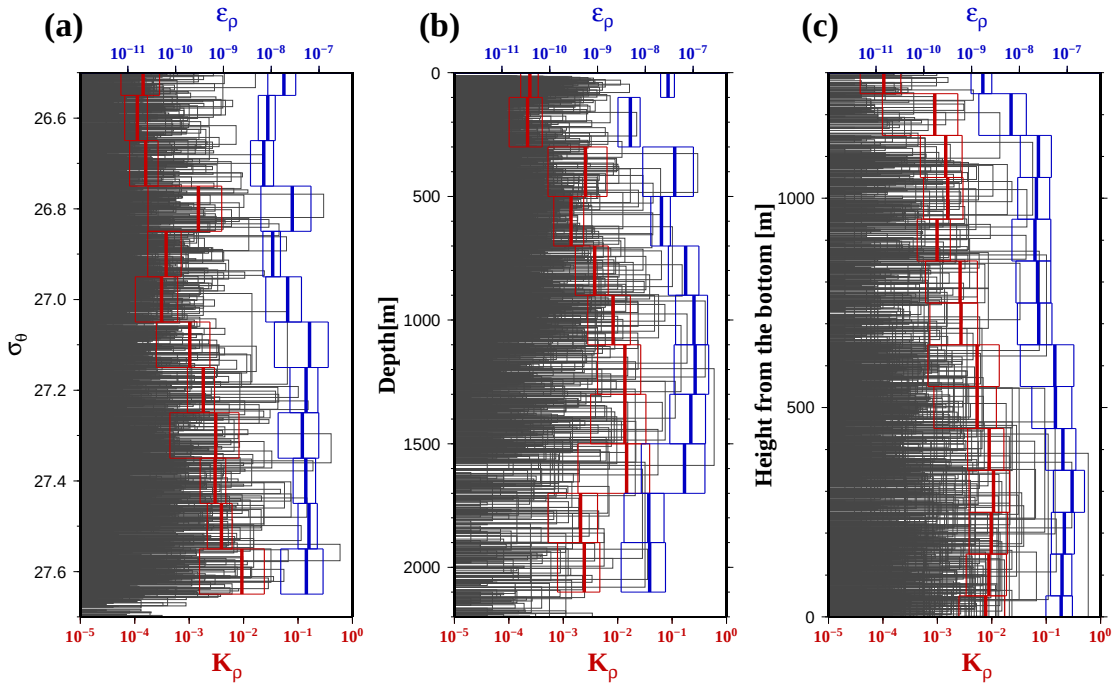


Figure 3.8 Distributions of K_ρ (in $m^2\,s^{-1}$) as a function of (a) potential density, (b) depth from the surface, and (c) height from the bottom, based on all the density inversions during the *XP01* cruise (black lines). Thick red and blue lines indicate the median of K_ρ and ϵ_ρ (in $W\,kg^{-1}$), respectively, at intervals of (a) $0.1\,\sigma_\theta$, (b) 200 m, and (c) 100 m, with the two outer thin lines representing the 95% confidence interval as determined by the bootstrap method.

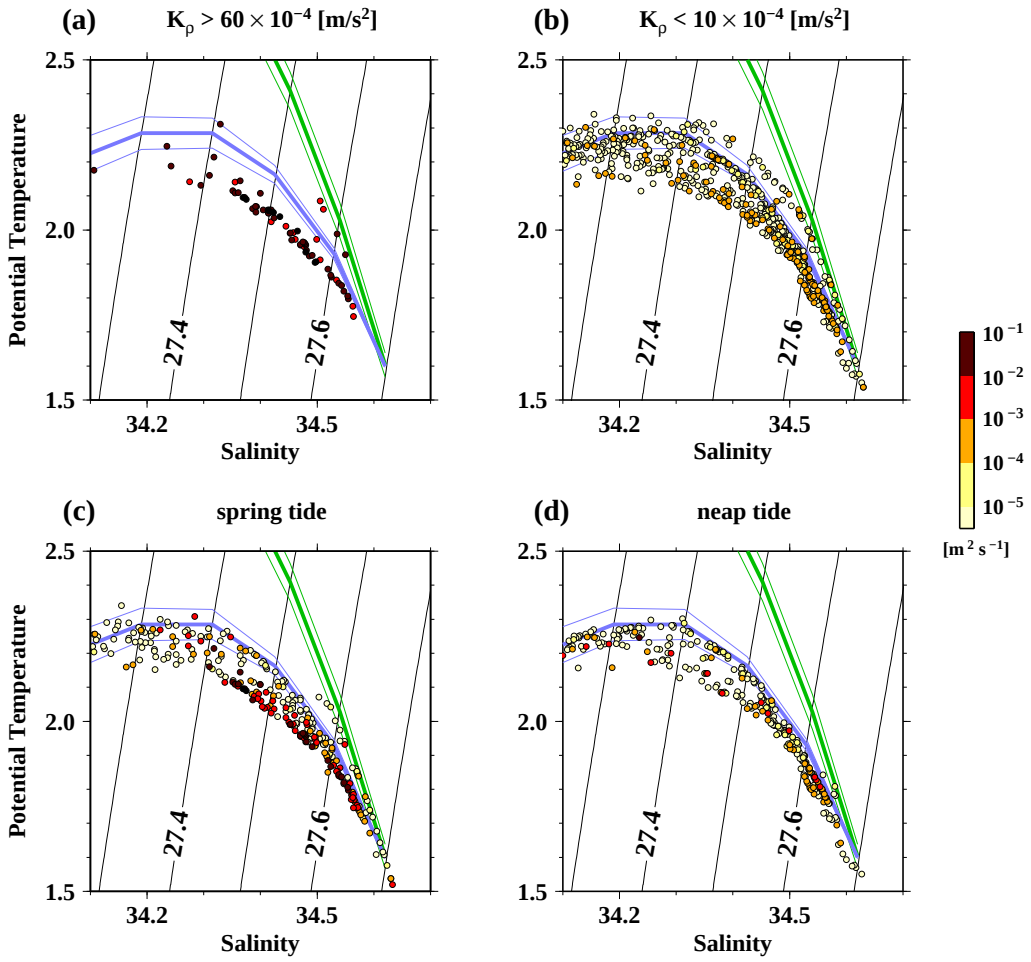


Figure 3.9 Potential temperature-salinity plots in the Bussol′ Strait for K_ρ values of (a) $> 50 \times 10^{-4}\,\mathrm{m^2\,s^{-1}}$ and (b) $< 10 \times 10^{-4}\,\mathrm{m^2\,s^{-1}}$, and at (c) spring tide and (d) neap tide. The plots are done at the depth intervals of 100 m from all the CTD data taken during *XP01*. The values of K_ρ are color-coded. The mean properties of EKCW (green lines) and KBW (blue lines) are also shown, with their standard deviation of potential temperature by $0.1\,\sigma_\theta$. The stations used for calculating the mean properties of EKCW and KBW are shown in Fig. 3.1.

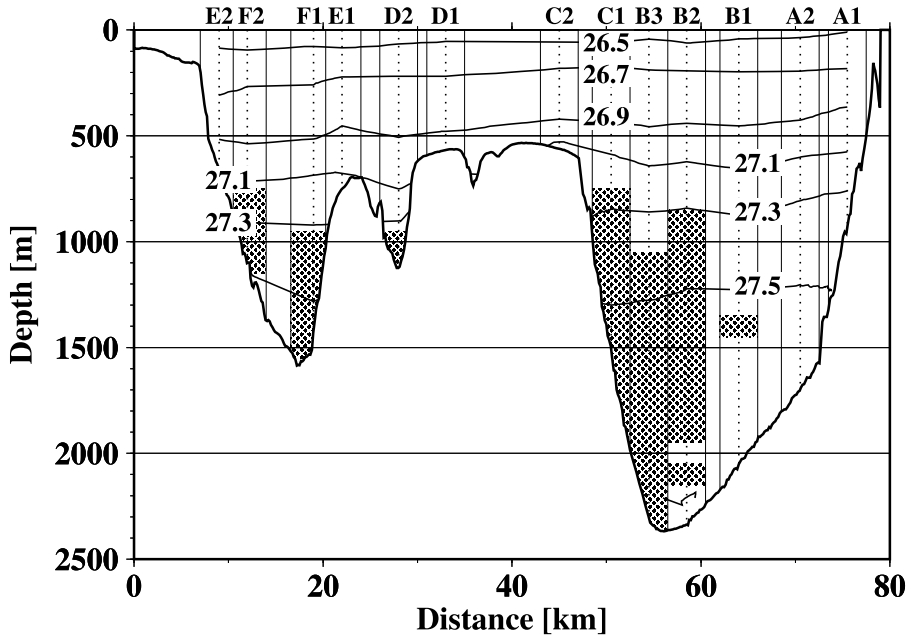


Figure 3.10 Spatial distribution of the unique colder and less-saline water characterized in the Bussol′ Strait at spring tide. The stippled areas represent water with a potential temperature lower than the mean KBW value minus its standard deviation on potential density surfaces.

Table 3.1 Summary of the performance of the quality tests and estimated quantities of vertical mixing for 13 stations in the Bussol′ Strait during *XP01*. Numbers of (a) CTD casts, (b) density inversions without the two quality control tests, (c) density inversions that passed the run-length test, and (d) density inversions that also passed the water mass test. We also list the (e) maximum length of the Thorpe scale, (f) maximum K_ρ, (g) maximum ϵ_ρ, (h) depth-averaged K_ρ, and (i) depth-averaged ϵ_ρ. Note that results for both spring and neap tides are listed for Stations B1, B2, B3, C2, F1, and F2.

Station	(a)	(b)	(c)	(d)	(e)	(f)	(g)	(h)	(i)
						$\times 10^{-4}$	$\times 10^{-9}$	$\times 10^{-4}$	$\times 10^{-9}$
					m	$m^2\,s^{-1}$	$W\,kg^{-1}$	$m^2\,s^{-1}$	$W\,kg^{-1}$
A1	7	487	234	188	69.9	3000	4700	120	180
A2	7	874	324	244	36.7	550	390	12	10
B1	6	785	271	207	18.4	120	210	1.7	1.9
B1(neap)	6	916	237	141	12.3	44	660	0.42	0.57
B2	6	938	353	271	24.2	240	250	3.8	2.9
B2(neap)	6	987	289	195	11.9	47	3500	0.41	1.6
B3	6	704	335	282	42.4	750	880	53	48
B3(neap)	6	890	299	180	9.8	31	490	0.79	0.71
C1	8	856	372	269	135.6	5900	2600	210	110
C2	8	477	159	105	7.8	32	240	1.2	4.3
C2(neap)	7	464	138	69	4.7	38	1600	0.42	5.3
D1	7	430	136	81	9.2	43	1600	2.6	8.6
D2	7	640	258	182	61.0	1500	4300	48	140
E1	6	482	149	112	14.8	110	1100	3.2	13
E2	7	299	181	141	21.7	220	410	12	30
F1	7	761	313	235	91.4	4000	4100	170	180
F1(neap)	6	842	246	178	47.7	1140	1200	21	27
F2	7	696	338	254	27.2	445	1300	19	44
F2(neap)	7	798	269	174	15.2	88	320	2.1	3.4
all	127	13,326	4901	3508	135.6	5900	4700	60	50

Chapter 4

General summary and conclusion

The Bussol′ Strait is a main conduit of water exchange between the Sea of Okhotsk and the Pacific. Furthermore, this strait is also a central site for water mass formation due to strong tidal mixing. Some numerical model studies have suggested that strong vertical mixing in the Kuril Straits has a substantial impact on the water mass distributions and thermohaline circulation in the North Pacific. It is therefore important to examine the water mass properties in the Bussol′ Strait and evaluate the vertical diffusivity there.

In 2001, under the international Japan-Russia joint study of the Sea of Okhotsk, intensive CTD/LADCP observations were performed at 13 stations across the Bussol′ Strait (*XP01*). These observations were provided the mean velocity, temperature, and salinity data in the Bussol′ Strait for the first time. In this study, we have used highly densed CTD/LADCP observation data taken by *XP01*.

In Chapter 2, we have revealed the features of water mass exchange between the Sea of Okhotsk and the Pacific through the Bussol′ Strait, using *XP01* data. In addition to the analysis of *XP01* data, we have created a retrospective data set in the region around the Bussol′ Strait from all available hydrographic data. In the density range of 27.3–27.6σ_θ (approximately 1000–1800 m), part of the water in the strait is colder, less-saline, and has higher dissolved oxygen concentration than both KBW and EKCW. On the other hands, potential vorticity profile (Fig. 2.5) suggests relatively intense diapycnal mixing in the Bussol′ Strait and also the production of water masses with density around 26.8σ_θ. On the basis of XCTD observation crossing the Bussol′ Strait from the Sea of Okhotsk to the

Pacific, we have found followings: the water in the intermediate layer in the Bussol′ Strait, which has a property nearly identical to KBW, forms the water mass front with EKCW. This water mass front corresponds to the front of the Oyashio Current. Furthermore, the front is advected back and forth near the strait by the strong tidal current. Our analyses of water mass properties also suggest that strong vertical mixing occurs in the vicinity of the Bussol′ Strait. Around the strait, the seasonal change of water mass properties can be identified up to the $26.8\sigma_\theta$ layer, to which winter convection cannot reach directly. We propose that combination of winter convection and strong diapycnal mixing leads to an effective ventilation of the intermediate layer. Through this combination mechanism interannual variability of the winter cooling would possibly penetrate into the intermediate water.

In Chapter 3, we have estimated vertical diffusivity in the Bussol′ Strait, with the focus being on vertical structure. We found the vigorous density inversions occurred in the strait with the largest vertical displacement being over 250 m. To estimate the vertical length scale of overturns (Thorpe scale), we adopted the method of Galbraith and Kelley (1996) to identify 'real' density inversion (Appendix A). The vertical average of K_ρ estimated from all the CTD casts is $60 \times 10^{-4}\,\mathrm{m^2\,s^{-1}}$, using a bootstrap technique (Appendix B). Overall, K_ρ is relatively small in the upper 300 m, whereas it is relatively large below a depth of 500 m. The implication is that strong vertical mixing does not reach the sea surface, resulting in a double-celled thermohaline circulation in the North Pacific, according to Kawasaki and Hasumi (2010). The distributions of K_ρ and the amplitude of the diurnal tidal current are similar. There is some correlation between K_ρ and the amplitude of the diurnal tidal current ($r = 0.50$). Furthermore, we have proposed an empirical relationship between K_ρ and the amplitude of the diurnal tidal current (Eq. 3.5). We also found that K_ρ and ϵ_ρ differed by almost one order of magnitude during the spring and neap tides. This difference suggests that there is extremely large variability of tidal mixing during the fortnightly tidal cycle in and around the Kuril Straits. This variation might further induce the phenomena and circulation with a fortnightly cycle.

In the Bussol′ Strait, we found the unique water mass properties in the density range of 27.1–27.6 σ_θ which is colder, less-saline, and has higher dissolved oxygen concentration than both KBW and EKCW. These properties cannot be explained by simple isopycnal mixing between KBW and EKCW. This unique water can be explained only by diapycnal mixing between adjacent layers. In Chapter 3, we have examined the occurrence frequency of large K_ρ ($> 60 \times 10^{-4}\,m^2\,s^{-1}$) on potential temperature versus salinity plots for the case at spring and neap tide. Although the unique water mass occurs at both the spring and neap tide in the density range of 27.1–27.6 σ_θ, the occurrence frequency of $K_\rho > 60 \times 10^{-4}\,m^2\,s^{-1}$ was far more frequent during the spring tide than during neap tide. Furthermore, the unique water is distributed over the slope of the central seamount of the Bussol′ Strait (Fig 3.10), where intense vertical mixing occurs (Figs. 3.5a–d). These features suggest that the unique water is created locally in the strait by intense vertical mixing during spring tides, with the relatively large K_ρ over the slope of the central seamount of the strait.

Here we pay attention to the extent of the unique water mass away from the Bussol′ Strait. Crossing the Bussol′ Strait from the Sea of Okhotsk to the Pacific, based on XCTD data of *XP01* (Fig. 2.6), the unique water is found only at one station close to the Bussol′ Strait (not shown). At Station B5 on the Pacific side (see Figs. 2.1b and 2.6 for the location), part of the water shifts to the unique water mass property in the density of $\sim$27.4 σ_θ (drawn in black lines on Fig. 2.7a). This suggests that the extent of the unique water is confined in the vicinity of the strait, but likely advected back and forth near the strait by the strong tidal current. Although, this result is based only on the data of *XP01*. We therefore need a wide areal survey around the Bussol′ Strait using high-resolution CTD to reveal the general feature of the water mass extent and formation. Furthermore, long-term measurements such as mooring also obtains a better understanding of the relationship between the unique water mass and strong diurnal tidal current. Discussing these points will be important for the future work.

The present study advanced our understanding of vertical mixing and water mass

formation in the Kuril Straits, and thus will contribute to understandings of the large-scale dynamics such as NPIW formation and thermohaline circulation.

Appendix A

Thorpe scale calculation and GK96 Method

Figure A1 is a schematic of an observed potential density profile (gray line) with an overturn and its reordered profile (black line). The reordered profile is made by reordering the potential density into a gravitationally stable profile in the range of overturning. The vertical displacement scale (Thorpe displacement) (Dillon, 1982) can be calculated by comparing the observed and reordered potential density profiles as shown in the right panel of Fig. A1. The Thorpe scale is in fact the root mean square (rms) value of the Thorpe displacement over the reordering region. However, these signals include noise with a random frequency and random amplitude. The signals also include systematic noise caused by the mismatch in time response of the CTD temperature and conductivity sensors. GK96 proposed a scheme to identify a true density inversions caused by overturning of water parcels. Suspicious density inversions are eliminated by the following two tests.

First, we eliminate the overturns caused by random noise by a run-length test. Difference of the observed and reordered profiles $\rho' = \rho(\mathrm{z}) - \hat{\rho}(\mathrm{z})$, called as the Thorpe fluctuation, varies between positive and negative in turn. A depth interval within which the sign of ρ' does not change is defined as a 'run' (Fig. A1). In the case of random noise with a unit length of one, the probability for a run of length n is given by $P(n) = 2^{-n}$ on the probability density function, as described in GK96. Furthermore, the rms of the run

(run-length) would be $(\sum_{n=1}^{\infty} 2^{-n} n^2)^{1/2} = \sqrt{6}$ in the case of random noise (Timmermans et al., 2003). Thus, in the case that the run-length is shorter than $\sqrt{6}$, that overturn would be indistinguishable from random noise and then eliminated. In our analysis the minimum run unit is assumed to be the CTD resolution of 0.2 m. Thus, overturns shorter than $\sqrt{6} \times 0.2 \approx 0.49$ m are eliminated in the run-length test.

Next, we eliminate the overturns due to systematic noise by a water mass test. This test eliminates noise caused by the mismatch of temperature and conductivity sensors. A systematic noise creates a distorted relationship between potential temperature and salinity. By assuming a linear relationship between density and temperature/salinity in the reordering region, overturns diverged widely from this relationship are removed. The specific method is as follows: first, in the reordering region we perform a linear least squares fit of temperature to the observed potential density. Second, we calculate the rms of the difference between the fitted potential density and the observed potential density. This rms is nondimensionalized dividing by the rms of the Thorpe fluctuation over the reordering region. Similar calculation is also made for salinity. Finally, the signals with a ratio exceeding 1.0 either for temperature or salinity are regarded as noise and deleted. A strict water mass test might sometimes reject a true density inversion, resulting in underestimation of K_ρ and ϵ_ρ value. We present the sensitivity of the vertical diffusivity coefficient to the water mass test in Appendix C.

The performance of each of the two tests is summarized for all stations in Table 3.1. Initially 13,326 inversions were detected, and 3508 (26%) of these were accepted as true overturns. In Chapter 3, we consider the overturns and their Thorpe scale after the two quality control tests.

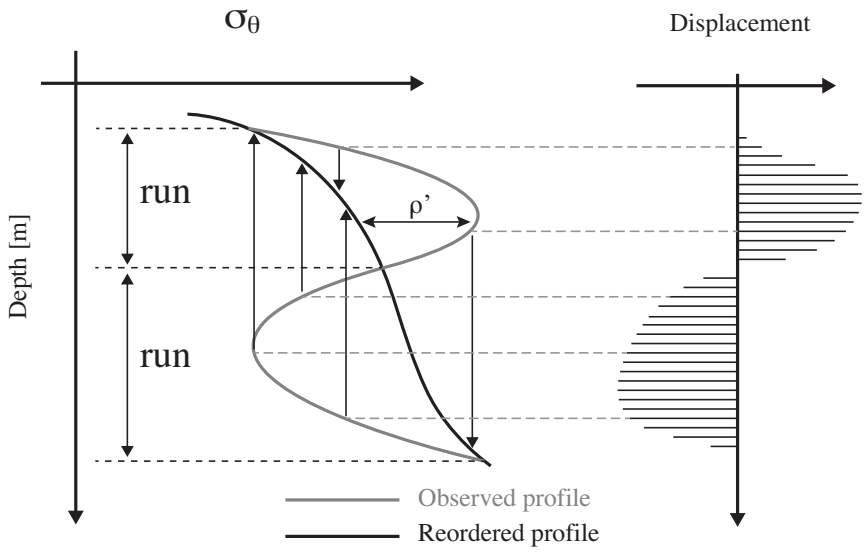


Figure A1 Schematics of an observed potential density profile (gray line) with an overturn and its reordered profile (black line) (left panel). The directions of the vertical arrows indicate the vertical displacements (Thorpe displacements). The right panel shows the profile of the Thorpe displacements.

Appendix B

Bootstrap Method

The bootstrap method (Efron and Gong, 1983) is a resampling method used to estimate the accuracy of calculated parameters. To estimate the accuracy of K_ρ and ϵ_ρ, previous studies have used the bootstrap technique (e.g., Fer et al., 2004; Ferrari and Polzin, 2005; Thompson et al., 2007). In this study procedures for averaging K_ρ and ϵ_ρ for each bin are as follows: (1) when the number of samples (casts) is n, random sampling with replacement is made n times, and then the sampled values are averaged: (2) this procedure is repeated 100,000 times, and then the probability density function of their averages (bootstrap distribution) is determined: (3) the median and confidence interval are calculated based on this bootstrap distribution. In Figs. 3.4 and 3.8, the error bars of K_ρ and ϵ_ρ are the 95% confidence intervals ($95th$ bootstrap percentiles). Confidence intervals were calculated based on 13 (neap tide) or 14 (spring tide) casts in Fig. 3.4 and 127 casts in Fig. 3.8. Figure B1 shows 90% confidence intervals calculated with the bootstrap method because the number of casts (6–9) is small.

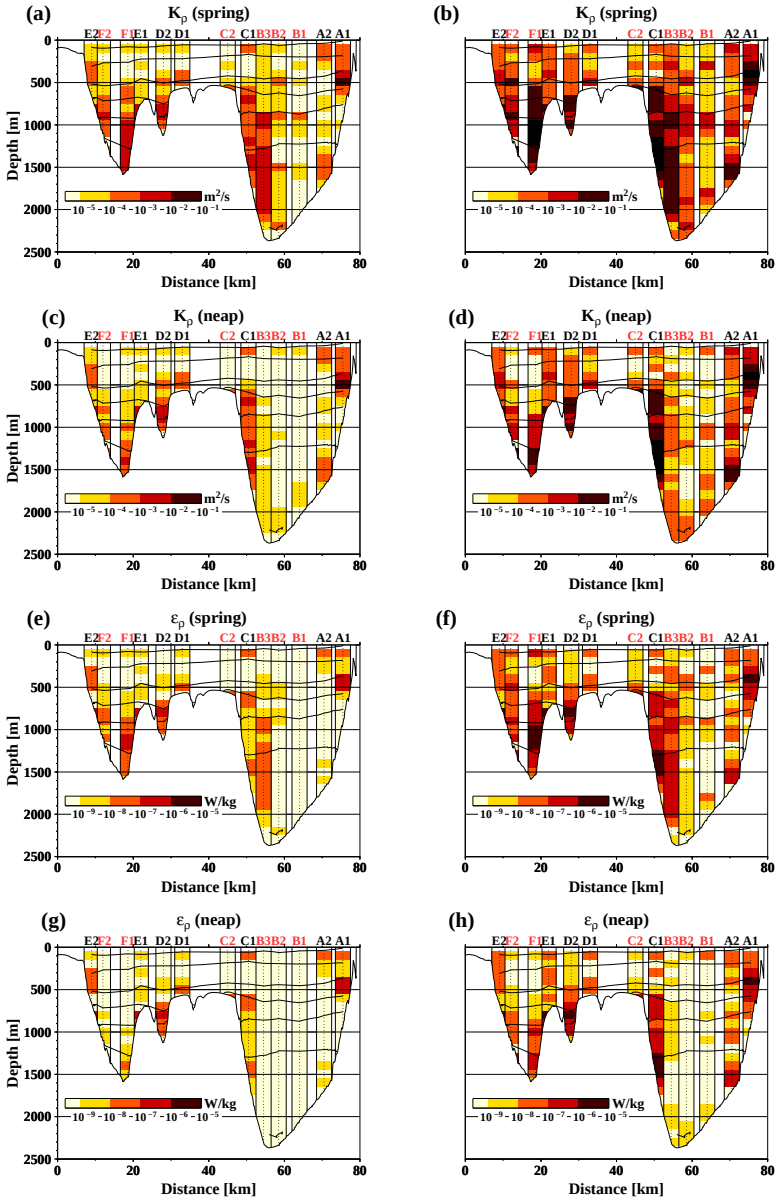


Figure B1 Ninety percent confidence intervals for Fig. 3.5. Intervals were calculated for all averages determined from 6–9 estimates by using the bootstrap method with 100,000 samples. The left column shows the lower confidence intervals and the right column shows the upper confidence intervals. The panels correspond to the cross-strait mapping of (a,b) K_ρ at spring tide, (c,d) K_ρ at neap tide, (e,f) ϵ_ρ at spring tide, and (g,h) ϵ_ρ at neap tide.

Appendix C

Sensitivity of the K_ρ estimation to the water mass test

Here we examine the sensitivity of the vertical diffusivity coefficient to the water mass test criterion. The strict criterion of 0.5 proposed by GK96 tends to reject some true overturns (e.g., Stansfield et al., 2001). Less strict criteria have therefore been used in several studies, such as 0.75 by Fer et al. (2004), and 2.0 by Martin and Rudnick (2007); Thompson et al. (2007). In this study we set the water mass test criterion to 1.0 as the baseline value. With the criterion set to 1.0, 3508 of 4901 (71%) inversions that passed the run-length test were accepted (Table 3.1). Adopting the less-stringent criterion of 2.0 leads to the acceptance of 4854 inversions (94%). Figure C1 shows K_ρ profiles with the criterion value of 1.0, 1.5, and 2.0 as a function of (a) potential density and (b) depth. K_ρ profiles are insensitive to the water mass test criterion except for the limited ranges of $< 26.7\,\sigma_\theta$ and $< 200\,\mathrm{m}$. Based on a total of 127 CTD casts with the criterion set to 1.5 and 2.0, the vertical averages of K_ρ were $65 \times 10^{-4}\,\mathrm{m^2\,s^{-1}}$ and $67 \times 10^{-4}\,\mathrm{m^2\,s^{-1}}$, respectively. These values are similar to the corresponding average K_ρ of $60 \times 10^{-4}\,\mathrm{m^2\,s^{-1}}$ with the criterion set to 1.0.

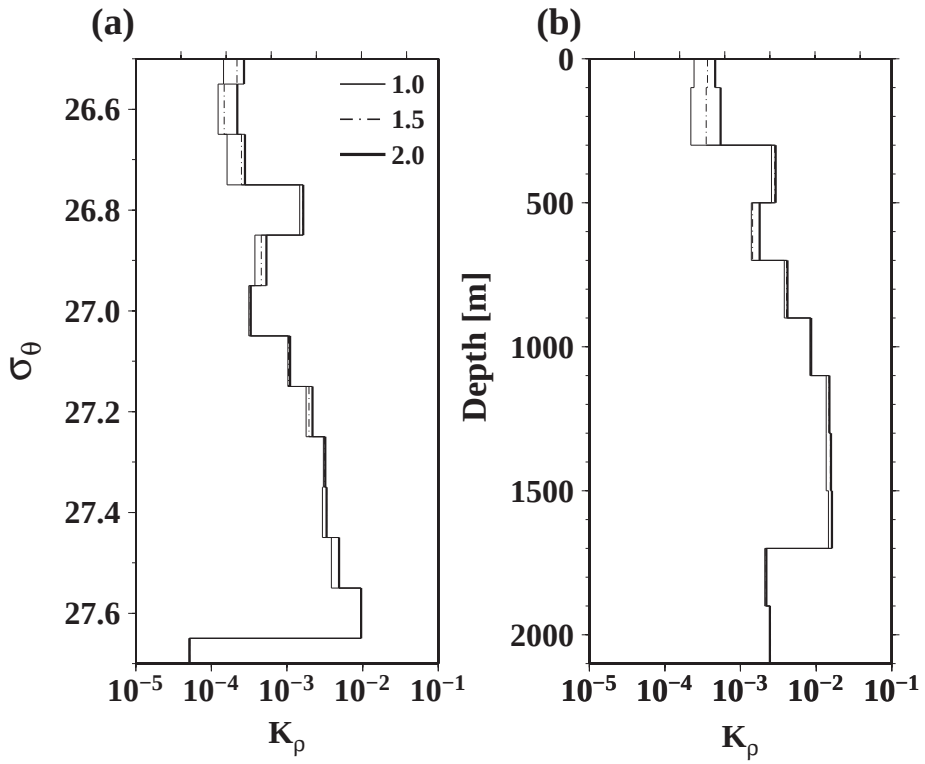


Figure C1 Vertical profile of median K_ρ values as a functions of (a) potential density and (b) depth, with the criteria of the water mass test being 1.0 (solid thin line), 1.5 (dotted line), and 2.0 (solid thick line).

Acknowledgments

First and foremost, I would like to express my deepest gratitude to Prof. Kay I. Ohshima for his instructive comments and useful suggestions. Unless I have participated in *XP01* cruise with him, I have never started to research an oceanography. He spent over 10 years to complete the dissertation with perpetual encouragement. I am most grateful to Prof. emeritus Masaaki Wakatsuchi for strong encouragement. He taught me about the importance of oceanography. I am deeply grateful to Dr. Yujiro Kitade (Tokyo University of Marine Science and Technology), Prof. Humio Mitsudera and Dr. Tomohiro Nakamura for reading the manuscript of the dissertation and providing useful comments and suggestions.

I am deeply indebted to the captain and crew of the R/V *Prof. Khromov*, and the principal investigators A. Scherbinin and S. Yarosh of the Far Eastern Regional Hydrometeorological Research Institute (Director Yuri N. Volkov), Russia, for their support during the observations. Thanks are extended to all the participants on the cruise for their collaboration. Hydrographical data of the dissertation were analyzed on the Pan-Okhotsk Information System of ILTS (I am an administrator of the system).

I would express my gratitude to colleagues of the technical division at ILTS for their encourage and support. Since I started working as a technical staff at ILTS, I've got a lot of precious experiences. First, I have participated in JARE52 (52nd Japan Antarctic Research Expedition). Dr. Yasushi Fukamachi gave me an opportunity to join in the expedition. I would greatly thank and acknowledge Dr. Jun Nishioka, Prof. Ichiro Yasuda and Yasuda laboratory's members, especially, Dr. Sachihiko Itoh, Dr. Yuki Tanaka, Dr. Satoshi Osafune, and Dr. Masahiro Yagi. We have joined in long-time observational

cruises including 4 times Russian cruises, and talked about enjoyable topics with some drinking. Furthermore, I would express my gratitude to all the faculty members at ILTS for continuous support.

My good friends since graduate school at DOAS (Division of Ocean and Atmospheric Science) have provided much friendship, emotional encouragement, and needed support, especially Dr. Taketo Hashioka, Dr. Shiro Nishikawa, Dr. Takeshi Tamura, Dr. Jun Ono, Dr. Kazuya Kusahara, Dr. Hideaki Ohtake, Dr. Rei Kudo, and Mr. Kousuke Ono. I would also thank to Ms. Kyoko Kitagawa for her encouragement and support.

I would like to express my deepest thanks to my parents and brother for their support. Finally, special thanks are expressed to my wife and son for their continuous encouragement and unflagging support.

References

Andreev, A., M. Honda, Y. Kuramoto, M. Kusakabe, and A. Murata, 2001. Excess CO_2 and pH excess in the intermediate water layer of the northwestern Pacific. J. Oceanogr., 57, 177–188.

Bulatov, N. V., L. A. Kurennaya, L. S. Muktepavel, M. G. Aleksanina, and E. E. Gerbek, 1999. Eddy water structure in the southern Okhotsk Sea and its seasonal variability (results of satellite monitoring). Oceanology 39, 29–37.

Crawford, W. R., 1986. A comparison of length scales and decay times of turbulence in stably stratified flows. J. Phys. Oceanogr. 16, 1847–1854.

Dillon, T. M., 1982. Vertical overturns: A comparison of Thorpe and Ozmidov length scales. J. Geophys. Res. 87, 9601–9613.

Efron, B., and G. Gong, 1983. A leisurely look at the bootstrap, the jackknife, and cross-validation. Am. Stat. 37, 36–48.

Fer, I., R. Skogseth, and P. M. Haugan, 2004. Mixing of the Storfjorden overflow (Svalbard Archipelago) inferred from density overturns. J. Geophys. Res. 109, C01005, doi:10.1029/2003JC001968.

Ferrari, R., and K. L. Polzin, 2005. Finescale structure of the T-S relation in the eastern North Atlantic. J. Phys. Oceanogr. 35, 1437–1454.

Ferron, B., H. Mercier, K. Speer, A. Gargett, and K. Polzin, 1998. Mixing in the Romanche fracture zone. J. Phys. Oceanogr. 28, 1929–1945.

Galbraith, P. S. and D. E. Kelley, 1996. Identifying overturns in CTD profiles. J. Atmos. Oceanic Technol. 13, 688-702.

Gladyshev, S., L. Talley, G. Khen and M. Wakatsuchi, 2003. Distribution, formation, and seasonal variability of Okhotsk Sea Mode Water. J. Geophys. Res., 108, 3186, doi:10.1029/2001JC000877.

Hibiya, T., M. Ogasawara, and Y. Niwa, 1998. A numerical study of the fortnightly modulation of basin-ocean water exchange across a tidal mixing zone. J. Phys. Oceanogr. 28, 1224–1235.

Itoh, M., K. I. Ohshima, and M. Wakatsuchi, 2003. Distribution and formation of Okhotsk Sea intermediate water: An analysis of isopycnal climatological data. J. Geophys. Res. 108, 3258, doi:10.1029/2002JC001590.

Itoh, S., I. Yasuda, T. Nakatsuka, J. Nishioka, and Y. N. Volkov, 2010. Fine- and microstructure observations in the Urup Strait, Kuril Islands, during August of 2006. J. Geophys. Res. 115, C08004, doi:10.1029/2009JC005629.

Itoh, S., I. Yasuda, M. Yagi, S. Osafune, H. Kaneko, J. Nishioka, T. Nakatsuka, and Y. N. Volkov, 2011. Strong vertical mixing in the Urup Strait. Geophys. Res. Lett. 38, L16607, doi:10.1029/2011GL048507.

Itsweire, E. C., 1984. Measurements of vertical overturns in a stably stratified turbulent flow. Phys. Fluids 27, 764–766.

Katsumata, K., K. I. Ohshima, T. Kono, M. Itoh, I. Yasuda, Y. Volkov, and M. Wakatsuchi, 2004. Water exchange and tidal currents through the Bussol′Strait revealed by direct current measurements. J. Geophys. Res. 109, C09S06, doi:10.1029/2003JC001864.

Kobayashi, T., 2000. Estimation of the freshwater transport and the water exchange through the passages of the Kuril Islands. Umi to Sora, 76, 25–32 (in Japanese).

Kawasaki, Y. and T. Kono, 1994. Distribution and transport of subarctic waters around the middle of Kuril Islands. Umi to Sora, 70, 71–84 (in Japanese).

Kawasaki, T., and H. Hasumi, 2010. Role of localized mixing around the Kuril Straits in the Pacific thermohaline circulation. J. Geophys. Res. 115, C11002, doi:10.1029/2010JC006130

Kitade, Y., M. Matsuyama, and J. Yoshida, 2003. Distribution of overturn induced by internal tides and Thorpe scale in Uchiura Bay. J. Oceanogr. 59, 845–850.

Kono, T., and Y. Kawasaki, 1997. Modification of the western subarctic water by exchange with the Okhotsk Sea. Deep Sea Res., 44, 689–711.

Lozier, S. M., W. B. Owens, and R. G. Curry, 1995. The climatology of the North Atlantic. Prog. Oceanogr., 36, 1 44.

Martin, J. P. and D. L. Rudnick, 2007. Inferences and observations of turbulent dissipation and mixing in the upper ocean at the Hawaiian Ridge. J. Phys. Oceanogr. 37, 476–494.

Moum, J. N., 1996. Energy-containing scales of turbulence in the ocean thermocline. J. Geophys. Res. 101, 14095–14109.

Nakamura, T., and T. Awaji, 2004. Tidally induced diapycnal mixing in the Kuril Straits and its role in water transformation and transport: a three-dimensional nonhydrostatic model experiment. J. Geophys. Res. 109, C09S07, doi:10.1029/2003JC001850.

Nakamura, T., T. Toyoda, Y. Ishikawa, and T. Awaji, 2006. Effects of tidal mixing at the Kuril Straits on North Pacific ventilation: Adjustment of the intermediate layer revealed from numerical experiments. J. Geophys. Res. 111, C04003, doi:10.1029/2005JC003142.

Nishioka, J., T. Nakatsuka, Y. W. Watanabe, I. Yasuda, K. Kuma, H. Ogawa, N. Ebuchi, A. Scherbinin, Y. N. Volkov, T. Shiraiwa, and M. Wakatsuchi, 2013. Intensive mixing along an island chain controls oceanic biogeohemical cycles. Global Biochem. Cycles. 27, 1–10, doi:10.1002/gbc.20088.

Ohshima, K. I., M. Wakatsuchi, Y. Fukamachi, and G. Mizuta, 2002. Near–surface circulation and tidal currents of the Okhotsk Sea observed with the satellite–tracked drifters. J. Geophys. Res. 107, 3195-3210, doi:10.1029/2001JC001005.

Ohshima, K. I., Y. Fukamachi, T. Mutoh, and M. Wakatsuchi, 2005. A generation mechanism for mesoscale eddies in the Kuril Basin of the Okhotsk Sea: baroclinic instability caused by enhanced tidal mixing. J. Oceanogr. 61, 247–260.

Ohshima, K. I., T. Nakanowatari, S. Riser, and M. Wakatsuchi, 2010. Seasonal variation in the in- and outflow of the Okhotsk Sea with the North Pacific. Deep Sea Res. II 57, 1247-1256, doi:10.1016/J.DSR2.2009.12.012.

Ono, T., Y. W. Watanabe, and K. Sasaki, 2000. Annual anthropogenic carbon transport into the North Pacific Intermediate Water through the Kuroshio/Oyashio interfrontal zone: An estimation from CFCs distribution. J. Oceanogr., 56, 675–689.

Ono, K., K. I. Ohshima, T. Kono, M. Itoh, K. Katsumata, Y. N. Volkov, and M. Wakatsuchi, 2007. Water mass exchange and diapycnal mixing at Bussol′ Strait revealed by water mass properties. J. Oceanogr. 63, 281–291.

Osborn, T. R., 1980. Estimates of the local rate of vertical diffusion from dissipation measurements. J. Phys. Oceanogr. 10, 83–89.

Ozmidov, R. V., 1965. On the turbulent exchange in a stably stratified ocean. Izv. Acad. Sci. U.S.S.R. Atmos. Oceanic Phys. 1, 861–871.

Reid, J. L., Jr. 1965. Intermediate waters of the Pacific Ocean. The Johns Hopkins Oceanogr. Stud., 2, 85 pp.

Reid, J. L. Jr., 1973. North Pacific Ocean Waters in Winter. The Johns Hopkins Oceanogr. Stud., 5, 96pp.

Riser, S. C., G. I. Yurasov, and M. J. Warner, 1995. Hydrographic and Tracer Measurements of the Water Mass Structure and Transport in the Okhotsk Sea in Early Spring.

PICES Sci. Rep. 2, edited by L. D. Tally and Y. Nagata, pp 138–143, Sidney, B. C., Canada.

Riser, S. C., 2001. The exchange of water between the Okhotsk Sea and the North Pacific Ocean, and implication to intermediate water formation. Proc. of Int. Symp. on Atmosphere-Ocean-Cryosphere Interaction in the Sea of Okhotsk and Surrounding Environment, Hokkaido Univ., Hokkaido.

Shcherbina, A., L. D. Talley, and D. L. Rudnick, 2003. Direct observations of North Pacific ventilation: brine rejection in the Okhotsk Sea. Science 302, 1952-1955.

Stansfield, K., C. Garrett, and R. Dewey, 2001. The probability distribution of the Thorpe Displacement within Overturns in Juan Ne Fuca Strait. J. Phys. Oceanogr. 31, 3421–3434.

Talley, L. D., 1991. An Okhotsk Sea water anomaly: implications for ventilation in the North Pacific. Deep Sea Res. 38, (Suppl.1), 171–190.

Talley, L. D., 1993. Distribution and formation of North Pacific Intermediate Water. J. Phys. Oceanogr., 23, 517–537.

Tanaka, Y., T. Hibiya, and Y. Niwa, 2007. Estimates of tidal energy dissipation and diapycnal diffusivity in the Kuril Straits using TOPEX/POSEIDON altimeter data. J. Geophys. Res. 112, C10021, doi:10.1029/2007JC004172.

Tanaka, Y., T. Hibiya, and Y. Niwa, 2010a. Assessment of the effects of tidal mixing in the Kuril Straits on the formation of the North Pacific Intermediate Water. J. Phys. Oceanogr. 40, 2569–2574, doi:10.1175/2010JPO4506.1.

Tanaka, Y., T. Hibiya, Y. Niwa, and N. Iwamae, 2010b. Numerical study of K_1 internal tides in the Kuril straits. J. Geophys. Res. 115, C09016, doi:10.1029/2009JC005903.

Tatebe, H., and I. Yasuda, 2004. Oyashio southward intrusion and cross-gyre transport related to diapycnal upwelling in the Okhotsk Sea. J. Phys. Oceanogr. 34, 2327–2341.

Thompson, A. F., S. T. Gille, J. A. MacKinnon, and J. Sprintall, 2007. Spatial and temporal patterns of small-scale mixing in Drake Passage. J. Phys. Oceanogr. 37, 572–592, doi:10.1175/JPO3021.1.

Thorpe, S. A., 1977. Turbulence and mixing in a Scottish loch. Philos. Trans. Roy. Soc. London 286A, 125–181.

Timmermans, M. L., C. Garrett, and E. Carmack, 2003. The thermohaline structure and evolution of the deep waters in the Canada Basin, Arctic Ocean. Deep Sea Res. I 50, 1305–1321, doi:10.1016/S0967–0637(03)00125–0.

Tsunogai, S., T. Ono, and S. Watanabe, 1993. Increase in total carbonate in the western North Pacific water and a hypotheses on the missing sink of anthropogenic carbon. J. Oceanogr. 49, 305–315.

Warner, M. J., J. L. Bullister, D. P. Wisegarver, R. H. Gammon, and R. F. Weiss, 1996. Basin–wide distributions of chlorofluorocarbons CFC–11 and CFC–12 in the North Pacific: 1985–1989. J. Geophys. Res. 101, C9, 20525–20542.

Watanabe, T., and M. Wakatsuchi, 1998. Formation of 26.8–26.9σ_θ water in the Kuril Basin of the Sea of Okhotsk as a possible origin of North Pacific Intermediate Water. J. Geophys. Res. 103, 2849–2865.

Wong, C. S., R. J. Matear, H. J. Freeland, F. A. Whitney, and A. Bychkov, 1998. WOCE Line P1W in the Sea of Okhotsk. 2. CFCs and the formation rate of intermediate water. J. Geophys. Res. 103, C8, 15625–15642.

Yagi, M, and I. Yasuda, 2012. Deep intense vertical mixing in the Bussol′ Strait. Geophys. Res. Lett. 39, L01602, doi:10.1029/2011GL050349.

Yagi, M., and I. Yasuda, 2013. A modified method for estimating vertical profiles of turbulent dissipation rate using inversions in the Kuril Straits. J. Oceanogr. 69, 203–214, doi:10.1007/s10872-012-0165-1.

Yamamoto-Kawai, M., S. Watanabe, S. Tsunogai, and M. Wakatsuchi, 2004. Chlorofluorocarbons in the Sea of Okhotsk: Ventilation of the intermediate water. J. Geophys. Res., 109, C9, doi:10.1029/2003JC001919.

Yasuda, I, 1997. The origin of the North Pacific Intermediate Water. J. Geohys. Res., 102, 893–909.

Yasuda, I., S. Kouketsu, K. Katsumata, M. Ohiwa, Y. Kawasaki, and A. Kusaka, 2002. Influence of Okhotsk Sea Intermediate Water on the Oyashio and North Pacific Intermediate Water. J. Geophys. Res., 107, 3237, doi:10.1029/2001JC001037.